

# Conformational analysis of Asn-linked oligosaccharides: implications in biological processes

Pradman K. Qasba, Petety V. Balaji, Vallurupalli S.R. Rao

*Structural Glycology Section, Laboratory of Experimental and Computational Biology, National Cancer Institute, National Institutes of Health,  
Bld: 469, Room 221, P.O. Box B, Frederick, MD 21702–1201, USA*

Received 11 December 1995; accepted 20 February 1996

---

## Abstract

Molecular dynamics simulations of several Asn-linked oligosaccharides carried out recently have been summarized. These oligosaccharides are flexible and the core  $\alpha 1 \rightarrow 3$ - and  $\alpha 1 \rightarrow 6$ -linkages play important roles in determining the overall shape of the molecule. The orientation of the  $1 \rightarrow 6$ -arm is affected not only by changes in  $\chi$  but also by changes in  $\phi$  and  $\psi$  around the  $\alpha 1 \rightarrow 6$ -linkage. The processing of  $\text{Man}_9\text{GlcNAc}_2$  to  $\text{Man}_5\text{GlcNAc}_2$  during the biosynthesis of Asn-linked oligosaccharides proceeds in well-defined 'conformation driven' pathways. These molecular dynamics studies rationalize spectroscopic and biochemical observations such as the rate of cleavage of  $\alpha 1 \rightarrow 2$ -linked mannoses by  $\alpha$ -mannosidases, the action of  $\beta$ - $1 \rightarrow 4$ -galactosyltransferase on biantennary oligosaccharides, and the binding affinities of oligosaccharide ligands to the asialoglycoprotein receptor. © 1997 Elsevier Science B.V.

*Keywords:* Conformation; Glycolipid; Glycoprotein; Molecular dynamics; Oligosaccharides; N-linked oligosaccharide processing

---

## 1. Introduction

### 1.1. Asn-linked oligosaccharides

Glycoproteins constitute an important class of biopolymers and are involved in many biological processes. Most oligosaccharide moieties of glycoproteins fall in one of two major classes, based on the type of linkage between the oligosaccharide and the protein: Asn-linked, where the oligosaccharide is linked to the side chain amide group of an asparagine residue through a *N*-glycosyl bond, and Ser/Thr-linked, where the oligosaccharide is linked to the side chain hydroxyl group of a serine or threonine residue through an *O*-glycosyl bond. (In some glycoproteins, saccharides are linked to protein through

amino acid residues other than Asn and Ser/Thr [1].) All the Asn-linked oligosaccharides have a common pentasaccharide core:  $\text{Man-}\alpha 1 \rightarrow 6(\text{Man-}\alpha 1 \rightarrow 3)\text{-Man-}\beta 1 \rightarrow 4\text{-GlcNAc-}\beta 1 \rightarrow 4\text{-GlcNAc-}\beta 1 \rightarrow \text{Asn}$  (Fig. 1). The terminal  $\alpha 1 \rightarrow 6$ - and  $\alpha 1 \rightarrow 3$ -linked mannose residues may carry additional residues such as mannose, *N*-acetylglucosamine, fucose, galactose, *N*-acetylgalactosamine, and sialic acid. Based on the nature of the residues present on the pentasaccharide core, Asn-linked oligosaccharides are further classified into three types: high mannose (only mannose residues), hybrid type (mannose residues on the  $\alpha 1 \rightarrow 6$ -mannose and other residues on the  $\alpha 1 \rightarrow 3$ -mannose) and complex type (residues other than mannose) (Fig. 1). Besides, the core pentasaccharide is often either fucosylated ( $\alpha 1 \rightarrow 3/6$ -linked to GlcNAc) or

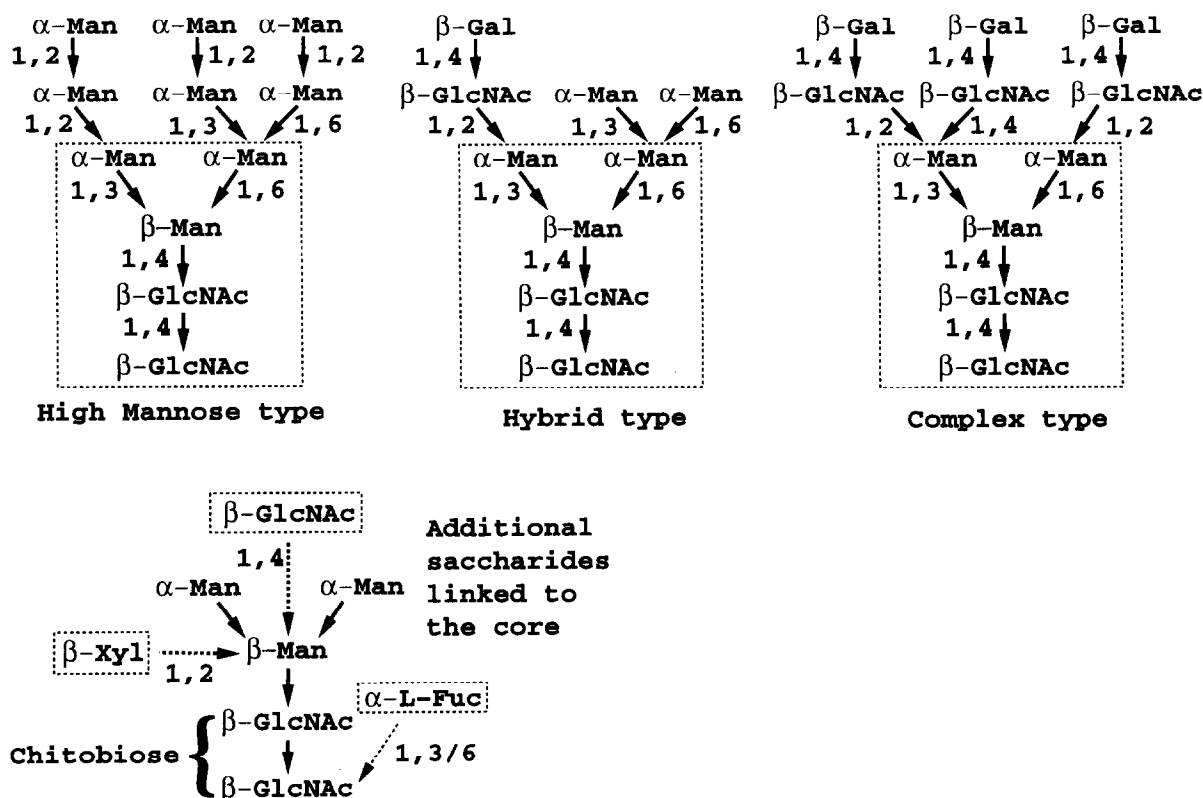


Fig. 1. Representative examples of the three types of Asn-linked oligosaccharides. The pentasaccharide core common to all three types is enclosed by dotted lines. The nature of the saccharides linked to the terminal  $\alpha 1 \rightarrow 3$ - and  $\alpha 1 \rightarrow 6$ -linked mannose residues of the core determines the type of oligosaccharide—high mannose, hybrid or complex. Besides these saccharides that are linked to the terminal mannoses, additional saccharides are also often found linked to the core: position and linkage types of such saccharides are shown.

xylosylated ( $\beta 1 \rightarrow 2$ -linked to middle mannose) and the hybrid and complex types are sometimes bisected ( $\beta 1 \rightarrow 4$ -GlcNAc on middle mannose). Saccharides of some glycoproteins are also either sulfated or phosphorylated. The presence or absence, and the type of Asn-linked oligosaccharides have been shown to play important roles in the biological function of many glycoproteins (see, for example, Refs. [2–7]).

## 2. Biosynthesis of Asn-linked oligosaccharides: overview

In the first step of protein *N*-glycosylation, a  $\text{Glc}_3\text{Man}_9\text{GlcNAc}_2$  precursor is transferred en bloc from the dolichol pyrophosphate donor to the Asn-residue of the nascent polypeptide chain (Fig. 2;

Ref. [8]). This co-translational event is followed by the processing of the precursor oligosaccharide by glycosidases and glycosyltransferases leading to various types of Asn-linked oligosaccharides. The three terminal glucose residues of the  $\text{Glc}_3\text{Man}_9\text{GlcNAc}_2$  precursor are removed by  $\alpha$ -glucosidases forming  $\text{Man}_9\text{GlcNAc}_2$  (M9; see Scheme 1) which is either left as such or is processed to different isomers of  $\text{Man}_8\text{GlcNAc}_2$  by specific  $\text{Man}_9$ -mannosidases [9]. One isomer of  $\text{Man}_8\text{GlcNAc}_2$  can also be generated directly without the prior formation of  $\text{Man}_9\text{GlcNAc}_2$  by an endomannosidase which converts  $\text{Glc}_{[1-3]}\text{Man}_9\text{GlcNAc}_2$  to  $\text{Man}_8\text{GlcNAc}_2$  [10].  $\text{Man}_8\text{GlcNAc}_2$  is further processed by  $\alpha 1 \rightarrow 2$ -linkage specific mannosidase(s) I to different levels forming other high-mannose type oligosaccharide intermediates which finally lead to  $\text{Man}_5\text{GlcNAc}_2$  (M5; Scheme 1). Next,

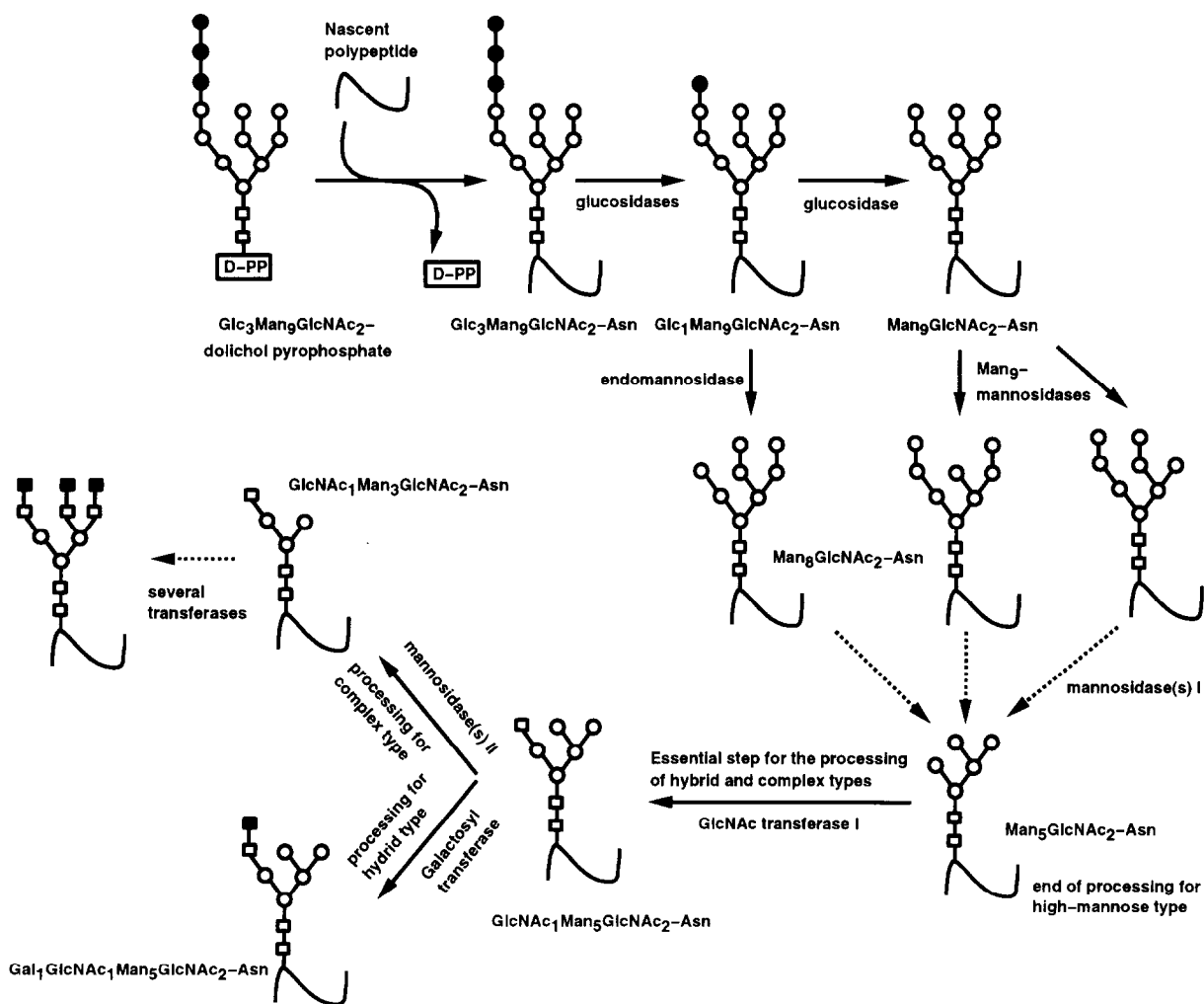
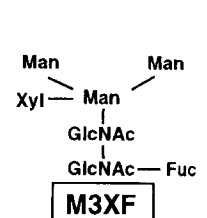
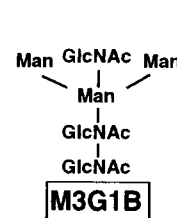
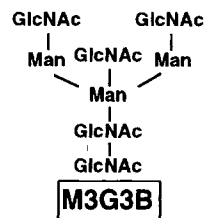
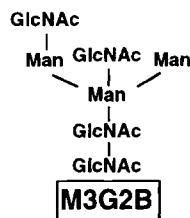
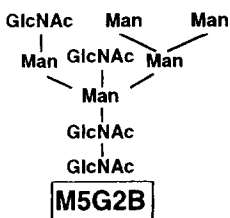
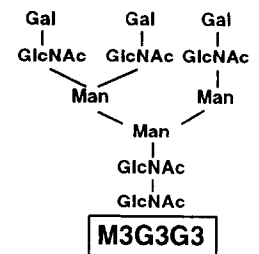
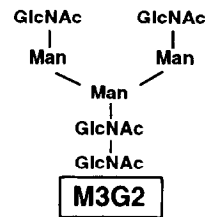
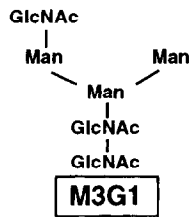
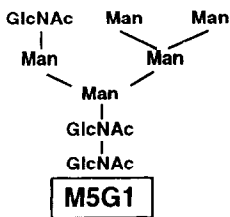
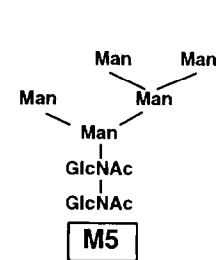
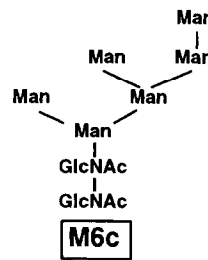
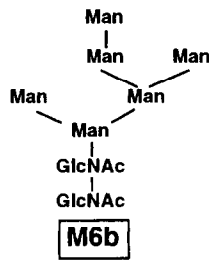
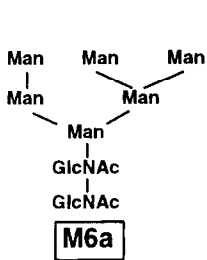
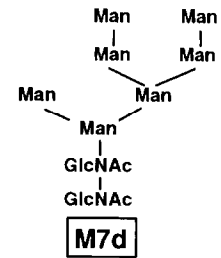
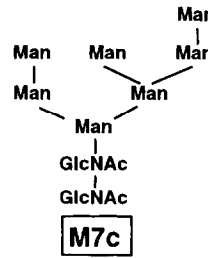
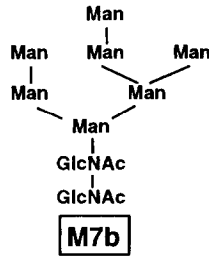
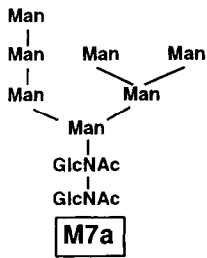
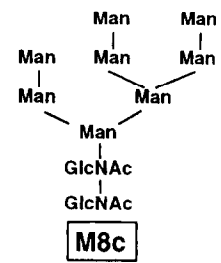
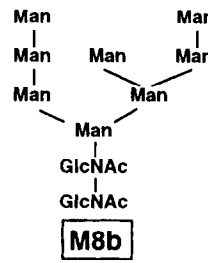
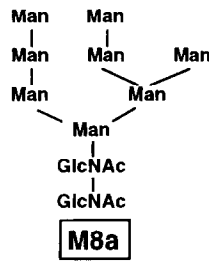
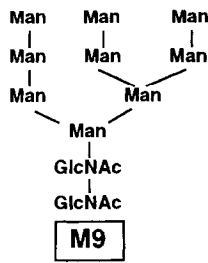


Fig. 2. Pictorial representation of the processing of Asn-linked oligosaccharides. Abbreviations and symbols used: D-PP, dolichol pyrophosphate donor; □, *N*-acetylglucosamine (GlcNAc); ○, mannose (Man); ●, glucose (Glc); ■, galactose (Gal). Solid arrows indicate a single step of processing whereas dotted arrows indicate multiple steps of processing.

GlcNAc transferase I transfers GlcNAc in  $\beta 1 \rightarrow 2$  linkage to the core  $\alpha 1 \rightarrow 3$ -mannose of  $\text{Man}_5\text{GlcNAc}_2$  to generate  $\text{GlcNAc}_1\text{Man}_5\text{GlcNAc}_2$ . Such an addition of GlcNAc is a necessary step for the biosynthesis of hybrid and complex type oligosaccharides (Fig. 2). From  $\text{GlcNAc}_1\text{Man}_5\text{GlcNAc}_2$ , either various hybrid oligosaccharides are generated by the concerted action of several glycosyltransferases or the complex type oligosaccharide biosynthesis is initiated with the action of  $\alpha$ -mannosidase(s) II. The  $\alpha$ -mannosidase II removes the terminal  $\alpha 1 \rightarrow 3$ - and  $\alpha 1 \rightarrow 6$ -linked mannose residues on the  $\alpha 1 \rightarrow 6$ -arm of  $\text{GlcNAc}_1$

$\text{Man}_5\text{GlcNAc}_2$  forming  $\text{GlcNAc}_1\text{Man}_3\text{GlcNAc}_2$ . This is a committed step in the biosynthesis of complex type oligosaccharides and this intermediate serves as the initial substrate to other glycosyltransferases such as GlcNAc-, Gal-, GalNAc-, Fuc- and Sialyl-transferases leading to the formation of diverse complex type oligosaccharides.

Even though the assembly and processing of Asn-linked oligosaccharides essentially follow the same pathways in many organisms, however, under conditions of glucose starvation and in some lower organisms like trypanosomatic protozoa, assembly and



processing of *N*-glycosylation has been shown to follow alternate pathways [11–13]. The factors responsible for the nature and type of the oligosaccharide present on the glycoproteins are still not very clear. The nature of the oligosaccharide at a glycosylation site for some glycoproteins is conserved in different species [14,15], whereas it differs in some other glycoproteins from one species to another [16,17]. In addition to the species dependency, the exact processing and hence the nature of the oligosaccharide has also been shown to depend on the tissue, developmental stage, the amino acid sequence of the entire protein (i.e. the three dimensional structure of the protein) and on the specificities and levels of the processing enzymes [18–21]. Interestingly, Hsieh et al. [22] showed that, of the two glycosylation sites of the Sindbis virus envelope glycoprotein E1, one site, regardless of the host cell type, has exclusively complex type oligosaccharides. However, the second glycosylation site has different types (high mannose or complex) of Asn-linked oligosaccharides in different host cells. Presently, more than one Man<sub>9</sub>-mannosidase has been identified in the ER and these enzymes have been shown to cleave different terminal mannoses of M9 i.e., they show different product specificities [23]. Using a mannosidase inhibitor, Kornfeld and coworkers showed that one of the ER resident Man<sub>9</sub>-mannosidases processes only about half of the glycoproteins [19]. Based on this and several other experimental observations, it was suggested that the processing of Man<sub>9</sub>GlcNAc<sub>2</sub> (M9) to Man<sub>5</sub>GlcNAc<sub>2</sub> (M5) by  $\alpha$ -mannosidase(s) I proceeds in well defined sequential pathways [24] and that the accessibility and conformation of the oligosaccharides play important roles in determining these processing steps. Spatial and steric considerations of the oligosaccharide ligands are important in determining the modes of binding and for glycosyltransferase action [25]. Hence, a clear understanding of these sequential pathways requires detailed information about the complexes of these oligosaccharide intermediates with glycosidases and glycosyltransferases. In the absence of the three dimensional structures of these enzymes, the conformations of just the oligosaccharide intermediates have been studied and the information

obtained from these studies has been correlated with the experimental data.

### 3. Conformation of oligosaccharides: the need for MD simulations

Among the various methods that are being used today, X-ray diffraction is perhaps the only method that gives information about the precise position of atoms and hence, about the three-dimensional structure of proteins and other molecules. Although a significant number of glycoprotein structures have been reported by X-ray crystallographic methods, only in a handful of these structures, the Asn-linked oligosaccharide has been completely traced beyond its core structure [26–32]. In all these structures, oligosaccharides have either been part of a glycoprotein or are complexed with the receptor protein and these studies gave information about one of the conformations accessible to the oligosaccharide. NMR spectroscopy in combination with molecular dynamics simulations has also been used to determine the probable conformations of some of the Asn-linked oligosaccharides [33,34]. However, the results derived from NMR studies correspond to the time averaged conformation since several conformers of an oligosaccharide exist in equilibrium in solution. As has been rightly pointed out earlier [35–37], the conformations of oligosaccharides when bound to proteins need not necessarily correspond to their equilibrium conformation in solution. In view of this, molecular dynamics (MD) simulations based on force field calculations serve as a very useful technique to obtain information about the accessible conformations of oligosaccharides. In fact, the conformation of the heptasaccharide Man- $\alpha$ 1  $\rightarrow$  6[Man- $\alpha$ 1-3][Xyl- $\beta$ 1  $\rightarrow$  2]-Man- $\beta$ 1  $\rightarrow$  4-GlcNAc- $\beta$ 1-4[L-Fuc- $\alpha$ 1  $\rightarrow$  3]-GlcNAc (linked to Asn 17 of *Erythrina corallodendron* lectin subunits) observed in the crystal [31] is also accessed in the MD simulations even though this is not the preferred conformation for the isolated heptasaccharide [38]. Hence, the probable conformations of several Asn-linked oligosaccharides (Scheme 1) that either are a part of glycoproteins or are possible

intermediates during the biosynthesis, have been recently studied by the MD simulations [38–41], and these results are summarized below (Section 5). The information obtained from these studies has also been used to explain/rationalize some of the experimental observations (Section 6). In conclusion, a pathway for the possible processing of Man<sub>9</sub>GlcNAc<sub>2</sub> to Man<sub>5</sub>GlcNAc<sub>2</sub> during the biosynthesis

of Asn-linked oligosaccharides has been proposed using the available experimental and computational data [40].

#### 4. Calculation procedure

All the calculations were performed on the National

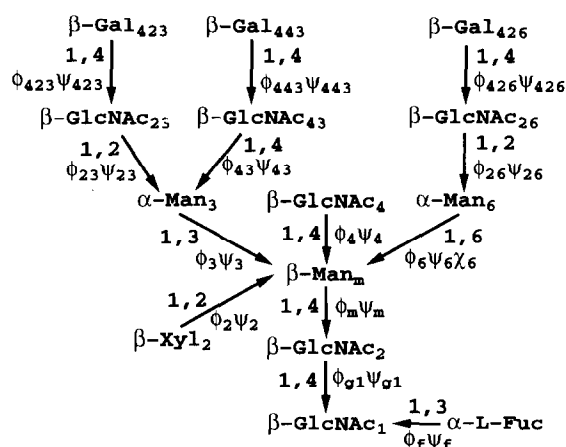
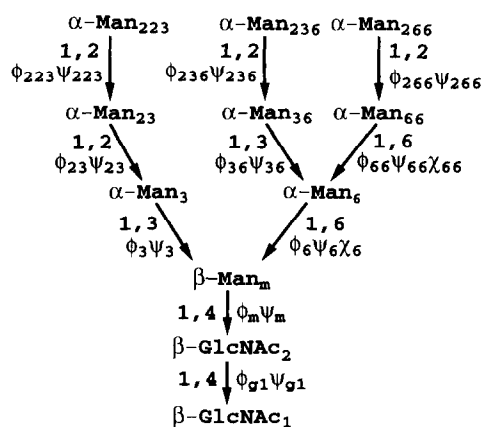
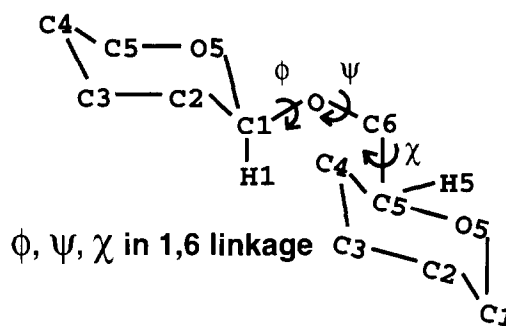
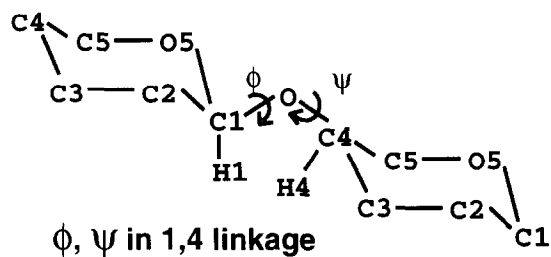
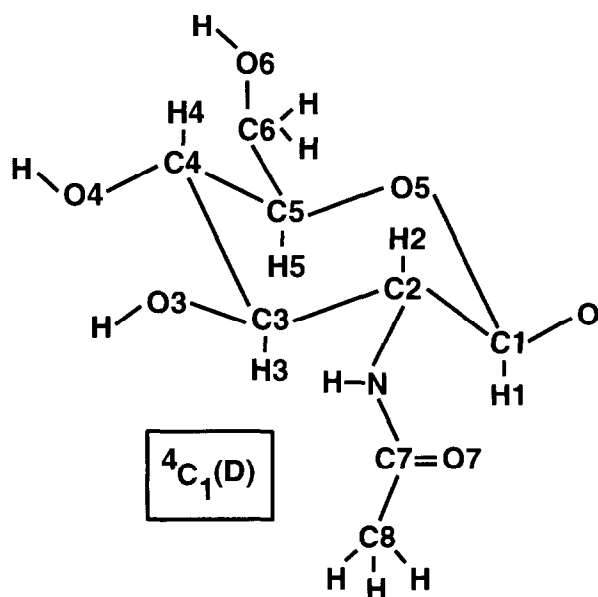


Fig. 3. Schematic diagram showing the atom names and torsion angle definitions used in the present study. All the saccharides are  ${}^4C_1(D)$  pyranosides except fucose which is  ${}^1C_4(L)$ .  $\phi$  and  $\psi$  in 1 → 2-, 1 → 3- and 1 → 4-linkages are defined as H1–C1–O–CX and C1–O–CX–HX respectively where CX and HX are the aglyconic atoms and O is the glycosidic oxygen.  $\phi$ ,  $\psi$ , and  $\chi$  in 1 → 6-linkage are defined as H1–C1–O–C6, C1–O–C6–C5 and O–C6–C5–H5 respectively.

Cancer Institute's Cray Y-MP 8D/ 8128 supercomputer using Biosym's Insight II and by considering all the atoms explicitly. The coordinates were first generated using IMPAC (interactive modeling package for carbohydrates) developed by P. Sailaja, P.V. Balaji, B. Vijaya Sai Reddy and V.S.R. Rao at the Molecular Biophysics Unit, Indian Institute of Science, Bangalore, India by taking the initial interglycosidic torsion angles  $\phi$ ,  $\psi$  and  $\chi$  (Fig. 3) from disaccharide  $\phi, \psi$  maps and energy minimization studies [42–46]. The initial structures so generated were subjected to energy minimization by the Newton–Raphson method until the maximum derivative was less than  $0.001 \text{ kcal mol}^{-1} \text{ \AA}^{-1}$ . Neither an explicit hydrogen bond potential nor any distance cut-offs were considered while calculating non-bonded interactions. A distance dependent dielectric constant of  $4*r$  was used for calculating electrostatic interactions. The minimized structures were subjected to an initial equilibration of 40 ps which was followed by a productive run (1000–3500 ps). All the calculations were in vacuo constant energy simulations carried out at a temperature of 300 K. Verlet's leap-frog algorithm was used for integration (time step = 1 fs). Simulations were also done with different seed values for the random number generator so that

different sets of initial velocities were assigned, leading to different trajectories from the same minimized conformation. The CVFF force field supplied with Biosym's Discover package was used in these studies. From the MD trajectories of the Man- $\alpha$ 1  $\rightarrow$  3-Man disaccharide, relative nuclear Overhauser effect (NOE) values relevant to the glycosidic linkage were calculated [38]. These back calculated theoretical NOE values were found to be in good agreement with the experimental values (Table 1), implying that the CVFF force field is reasonable and can be used in the conformational analysis of carbohydrates to the extent of determining the accessible conformations of the oligosaccharides.

## 5. Conformation of the Asn-linked oligosaccharides

### 5.1. Nomenclature

The oligosaccharides have been identified by the number of mannose, *N*-acetylglucosamine (excluding those in the core chitobiose) and galactose residues that it contains (Scheme 1). For example, M9 denotes nine mannoses attached to the 2 core chitobiose

Table 1  
Comparison of back-calculated and experimental NOE values for Man- $\alpha$ 1  $\rightarrow$  3-Man<sup>a</sup>

NOE connectivity <sup>b</sup>	Relative NOE <sup>c</sup>										Ave. NOE	Expt. NOE <sup>e</sup>
	40–140 <sup>d</sup>	141–240	241–340	341–440	441–540	541–640	641–740	741–840	841–940	941–1040		
Man <sub>1</sub> :H1– Man <sub>1</sub> :H2	1.00	1.00	1.00	1.00	1.00	1.00	1.00	1.00	1.00	1.00	1.00	1.00
Man <sub>1</sub> :H1– Man <sub>2</sub> :H2	0.27	0.33	0.22	0.24	0.18	0.31	0.18	0.26	0.26	0.26	0.25	JD <sup>f</sup>
Man <sub>1</sub> :H1– -Man <sub>2</sub> :H3	1.28	1.24	1.37	1.27	1.34	1.31	1.35	1.36	1.42	1.24	1.32	1.63 $\pm$ 0.3
Man <sub>1</sub> :H5– Man <sub>2</sub> :H2	0.33	0.28	0.37	0.40	0.56	0.27	0.52	0.41	0.42	0.35	0.39	0.54 $\pm$ 0.1

<sup>a</sup> NOE values were back-calculated for discrete 100 ps intervals from the 1000 ps MD trajectory of Man- $\alpha$ 1,3-Man disaccharide (from Ref. [38]).

<sup>b</sup> Non-reducing mannose is referred to as Man<sub>1</sub> and the reducing mannose as Man<sub>2</sub>.

<sup>c</sup> Relative NOE values calculated using Biosym's NMR\_Refine module with a mixing time of 750 ms and a rotational correlation time of 0.85 ns. The relative NOEs were calculated with respect to the intraresidue NOE between Man<sub>1</sub>:H1 and Man<sub>1</sub>:H2 in that set of 100 ps interval, which is  $2.40 \pm 0.03$  in absolute NOE (%) values.

<sup>d</sup> ps interval.

<sup>e</sup> Experimental data taken from Rutherford et al. [74].

<sup>f</sup> JD, just detectable.

GlcNAc residues. Oligosaccharides which have the same number of mannose residues but differ in position and linkages, are further distinguished by an additional alphabet a, b, c, or d. For example M8a, M8b and M8c all contain eight mannoses linked to the core chitobiose residues but the position and linkages of the mannoses are different in the three oligosaccharides. The oligosaccharides M9, M8a, M8b, M8c, M7a, M7b, M7c, M7d, M6a, M6b, M6c and M5 have been referred to in Balaji et al. [40] with the prefix ‘G2’ (i.e. M9 as G2M9, M8c as G2M8c etc.). In complex and hybrid oligosaccharides, the presence of bisecting GlcNAc is indicated by the addition of alphabet ‘B’ at the end, e.g. in M3G3B, there are three mannoses and three GlcNAcs attached to the core chitobiose, and one of the three GlcNAcs is bisecting. The oligosaccharide M3G3C3 is the same as oligosaccharide #IV of Balaji et al. [39]. The oligosaccharides

M3XF and M3G1B are referred to as ‘heptasaccharide’ and ‘bisected hexasaccharide,’ respectively, in [38]. The letters X and F denote the presence of  $\beta 1 \rightarrow 2$  linked xylose and  $\alpha 1 \rightarrow 3$ -linked L-fucose residues, respectively.

For identifying the saccharide residues in Asn-linked oligosaccharides, the following nomenclature has been used (Fig. 3(a)). The middle mannose residue  $\beta 1 \rightarrow 4$ -linked to the core chitobiose (GlcNAc<sub>2</sub>- $\beta 1 \rightarrow 4$ -GlcNAc<sub>1</sub>) is termed Man<sub>m</sub>. Mannoses  $\alpha 1 \rightarrow 3$ - and  $\alpha 1 \rightarrow 6$ -linked to Man<sub>m</sub> are termed Man<sub>3</sub> and Man<sub>6</sub>, respectively, where the subscripts ‘3’ and ‘6’ denote linkage position. Since all the glycosidic linkages (1  $\rightarrow$  2-, 1  $\rightarrow$  3-, 1  $\rightarrow$  4-, and 1  $\rightarrow$  6-) are through C1, only the position of the second saccharide (i.e. 2, 3, 4, and 6) is used as a subscript. For the remaining saccharides, the first number in the subscript denotes the hydroxyl through which it is linked

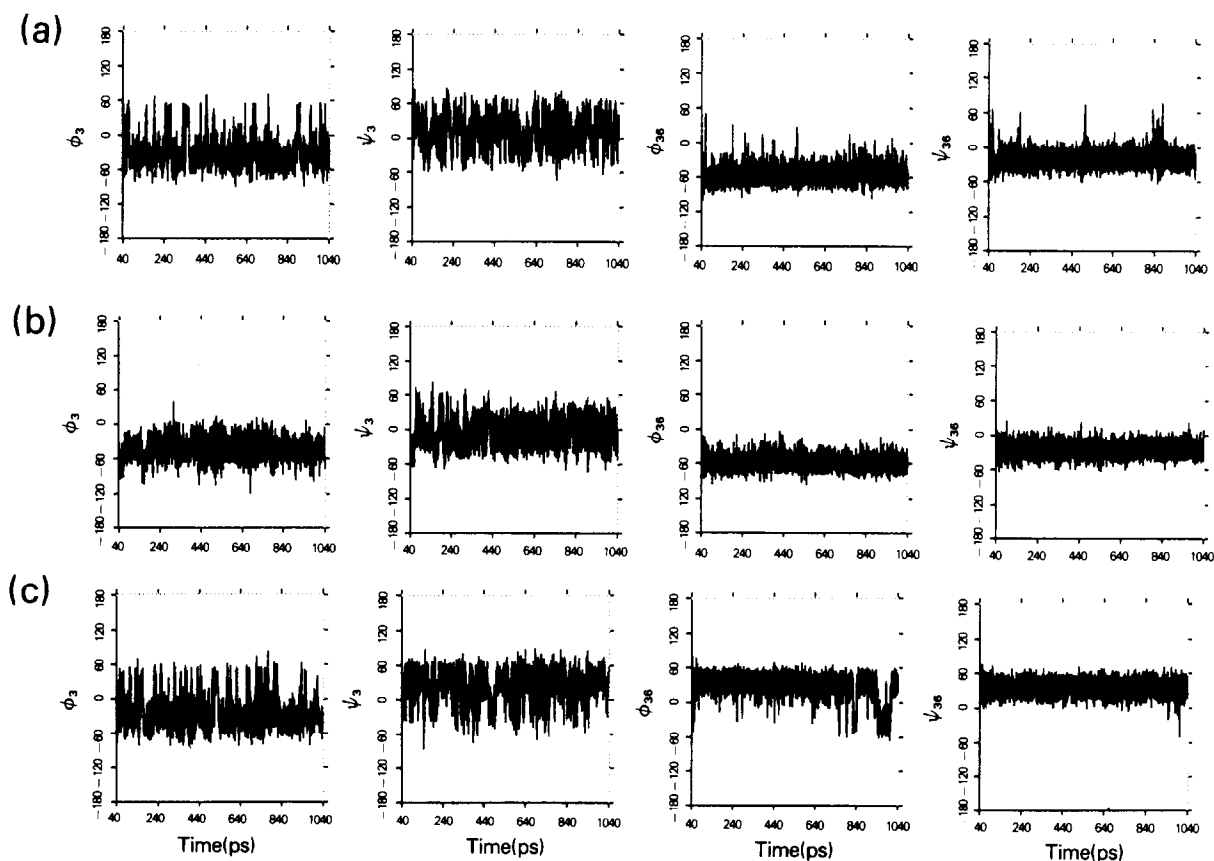


Fig. 4. Variation of the interglycosidic torsion angles around  $\alpha 1 \rightarrow 3$ -linkages. Torsion angle versus time plots for  $\phi_3, \psi_3$  and  $\phi_{36}, \psi_{36}$  extracted from the dynamics trajectories of (a) M7c, (b) M8a and (c) M8c (from Ref. [40]).

to the preceding residue. Numerals following the first number indicate how the preceding residue is linked up to  $\text{Man}_m$ . Hence, the last numeral in the subscript also indicates the 'arm' on which the residue is present. Thus,  $\text{Man}_{236}$  is the mannose residue 1  $\rightarrow$  2-linked to its preceding residue  $\text{Man}_{36}$  and both these residues are on the 1  $\rightarrow$  6-arm. The torsion angles are given the same subscript as the saccharide whose anomeric carbon is involved in the corresponding glycosidic linkage. The residue and torsion angle names used in Ref. [39] for M3G3G3 have been modified following the above convention.

### 5.2. $\alpha 1 \rightarrow 3$ -linkages

Conformation of the  $\text{Man}_{3-\alpha 1} \rightarrow 3\text{-Man}_m$  fragment plays an important role in determining the overall 'shape' of the Asn-linked oligosaccharides. In the MD simulations of the  $\text{Man-}\alpha 1 \rightarrow 3\text{-Man}$  disaccharide [38], both  $\phi$  and  $\psi$  fluctuate frequently between  $-60^\circ$  and  $+60^\circ$  suggesting that transitions between the different minimum energy conformations [47,48] take place easily and can be observed in the MD simulations. However, conformations corresponding to  $\psi$  around  $180^\circ$  were not accessed in any of the disaccharide simulations. Such conformations also were not observed in the Monte Carlo simulations of this disaccharide [49]. The fluctuations of  $\phi_3, \psi_3$  in all the oligosaccharides are similar to those observed

in the isolated disaccharide simulations except M7a, M8a, bisected hybrid, and bisected complex oligosaccharides (Fig. 4; Refs. [40,38]). In one of the simulations of the complex oligosaccharide M3G3G3, which has two antennae linked to  $\text{Man}_3$ , the fluctuations of  $\phi_3$  are even greater (from  $-80^\circ$  to  $+120^\circ$  [39]). MD simulations of the oligosaccharide M3XF show that the conformational fluctuations of  $\phi_3, \psi_3$  are not significantly affected by the  $\beta 1 \rightarrow 2$ -linked xylose residue [38]. In some of the simulations of complex oligosaccharides,  $\psi_3$  accesses a value around  $180^\circ$ .

In the high mannose type oligosaccharides, the  $\text{Man}_{36-\alpha 1} \rightarrow 3\text{-Man}_6$  fragment ( $\phi_{36}, \psi_{36}$ ) shows less flexibility than the  $\text{Man}_3-\alpha 1 \rightarrow 3\text{-Man}_m$  fragment ( $\phi_3, \psi_3$ ) (Fig. 4). This restriction on the fluctuations of  $\phi_{36}, \psi_{36}$  in the favored conformations is probably caused by the spatial proximity of  $\text{Man}_{36}$  to the core GlcNAc residues (Fig. 5). A comparison of the evolution of  $\phi_{36}$  and  $\psi_{36}$  during the 1000 ps simulation period in various high mannose oligosaccharides shows that the preferred values for these two angles are influenced by the presence of other saccharide residues and their conformations (Fig. 4). For example, in M8a (only  $\text{Man}_{236}$  present and not  $\text{Man}_{266}$ ; Scheme 1) and in M7c (only  $\text{Man}_{266}$  present and not  $\text{Man}_{236}$ ),  $\phi_{36}, \psi_{36}$  fluctuate around  $-60^\circ, -30^\circ$  whereas in M8c (both  $\text{Man}_{236}$  and  $\text{Man}_{266}$  are present),  $\phi_{36}, \psi_{36}$  fluctuate around  $30^\circ, 30^\circ$  (Fig. 4)—a change of about  $90^\circ$  and  $60^\circ$  in  $\phi_{36}$  and  $\psi_{36}$ , respectively. For the

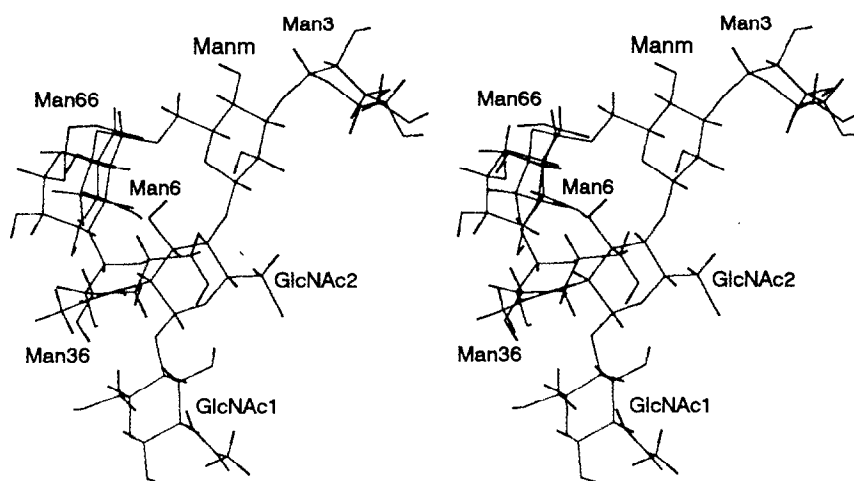


Fig. 5. Stereo view of one of the conformations of M5 accessed during the MD simulations (at 657 ps [40]) to show the proximity of  $\text{Man}_{36}$  to the core chitobiose residues and the exposure of  $\text{Man}_3$  to solvent and hence possibly to enzymes. Color codes used for stick diagram generated using Biosym's InsightII: carbon, green; oxygen, red; nitrogen, blue; hydrogen, black.

$\text{Man}_3\text{-}\alpha 1 \rightarrow 3\text{-Man}_m$  fragment, a hydrogen bond between  $\text{Man}_3\text{-O2}$  and  $\text{Man}_m\text{-O5}$  is possible when  $\phi_3, \psi_3$  is around  $-30^\circ, +30^\circ$ .

### 5.2.1. Effect of bis-GlcNAc on the conformation of $\text{Man}_3\text{-}\alpha 1 \rightarrow 3\text{-Man}_m$ fragment

Simulations of bisected hybrid and complex oligosaccharides show that in the presence of bis-GlcNAc, the conformational flexibility of the  $\text{Man}_3\text{-}\alpha 1 \rightarrow 3\text{-Man}_m$  fragment is restricted —

specifically the transitions of  $\phi_3$  to the positive region (i.e. values greater than  $0^\circ$ ) are either completely absent as in M5G2B or very infrequent as in M3G3B (Fig. 6 inset; Ref. [41]). Although similar conclusions were drawn from NMR studies, the reason for this effect was not clear [51]. Interestingly, in M3G1B, where  $\text{Man}_3$  is the terminal saccharide without any substitutions, the fluctuations of  $\phi_3, \psi_3$  were similar to those in an isolated  $\text{Man-}\alpha 1 \rightarrow 3\text{-Man}$  disaccharide [38]. This shows clearly that

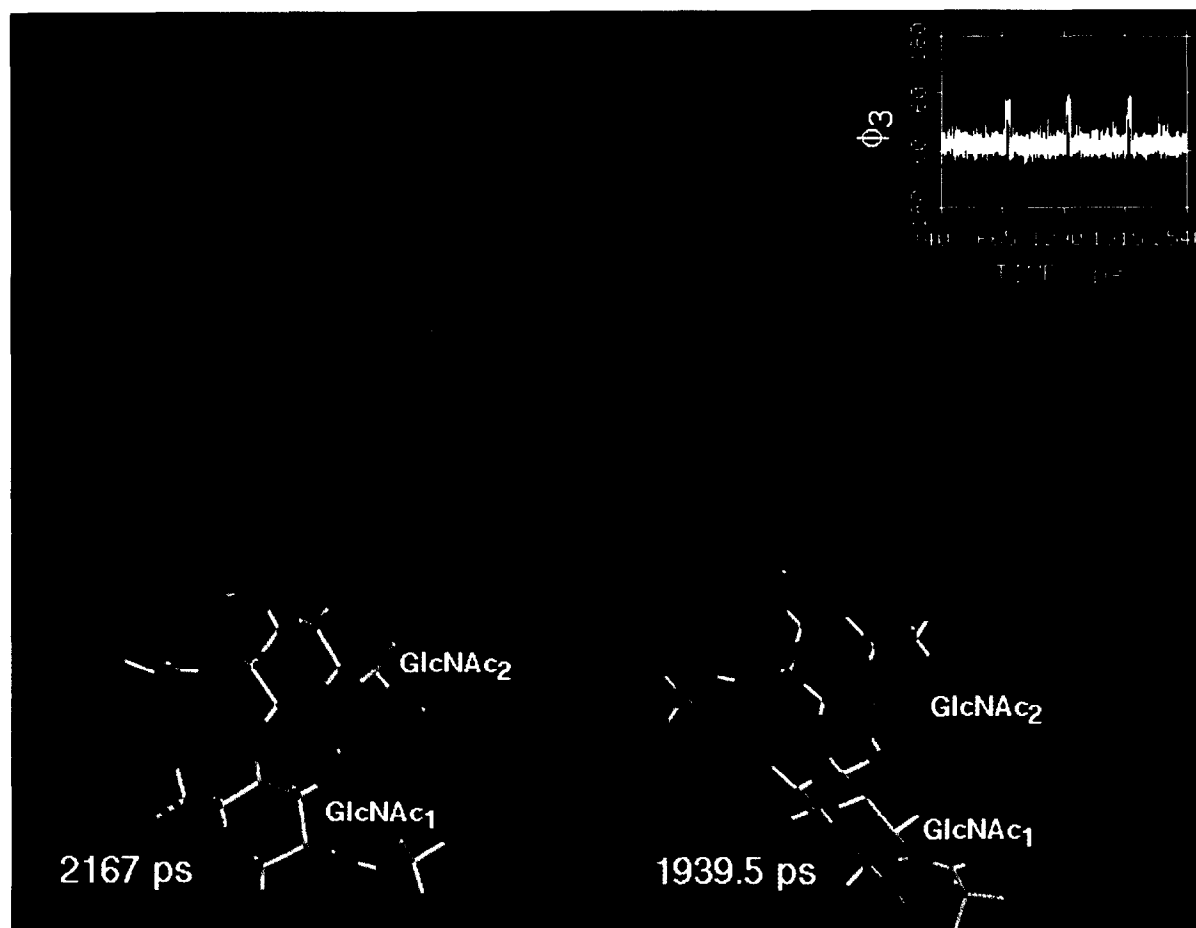


Fig. 6. Two of the conformations of M3G3B accessed during the MD simulations [41]. Conformations at 2167 ps (a; left) and 1939.5 ps (b; right), showing different orientations of  $\text{GlcNAc}_{23}$  relative to bis-GlcNAc,  $\text{GlcNAc}_4$ . The two conformers were first superposed by considering the C1, C3, C5 and O5 atoms of  $\text{Man}_m$  as reference atoms and were then separated to avoid spurious orientational differences.  $\phi_3, \psi_3$  are  $-62^\circ, -18^\circ$  and  $44.24^\circ$  in left (2167 ps) and right (1939.5 ps) conformations, respectively. Color code used: GlcNAc residues of the core chitobiose, white; trimannosidic core ( $\text{Man}_m$ ,  $\text{Man}_3$  and  $\text{Man}_6$ ), green; bisecting GlcNAc ( $\text{GlcNAc}_4$ ), brown; GlcNAcs linked to  $\text{Man}_3$  and  $\text{Man}_6$  ( $\text{GlcNAc}_{23}$  and  $\text{GlcNAc}_{26}$ ), yellow. Oxygen and nitrogen atoms are colored red and blue, respectively, in all the residues. All the color diagrams were drawn using MidasPlus software package [50]. Inset (top right): Torsion angle versus time plot for  $\phi_3$  extracted from the MD trajectories of M3G3B to show the occasional transitions of  $\phi_3$  from the preferred value of around  $-50^\circ$  to around  $45^\circ$ .

bis-GlcNAc dampens the fluctuations of  $\text{Man}_3\text{-}\alpha 1 \rightarrow 3\text{-Man}_m$  fragment only when a GlcNAc is  $\beta 1 \rightarrow 2$ -linked to  $\text{Man}_3$ . Whether similar effects are seen when GlcNAc is  $\beta 1 \rightarrow 4$ -linked to  $\text{Man}_3$  remains to be determined. As seen in one of the conformations of M3G3B (Fig. 6(a)) GlcNAc<sub>23</sub> and bis-GlcNAc are positioned 'face-to-face' and the hydrophobic interactions between these two residues probably stabilizes this conformation of the oligosaccharide leading to the dampening of the  $\text{Man}_3\text{-}\alpha 1 \rightarrow 3\text{-Man}_m$  fragment fluctuations. Thus the conformation corresponding to positive values of  $\phi_3$ , although stereochemically possible, is not preferred in the presence of bis-GlcNAc. However, M3G3B also occasionally accesses conformations in which GlcNAc<sub>23</sub> and bis-GlcNAc are not positioned 'face-to-face' (Fig. 6(b)).

### 5.3. $\alpha 1 \rightarrow 6$ -linkages

Similar to the  $\text{Man}_3\text{-}\alpha 1 \rightarrow 3\text{-Man}_m$  fragment of the core pentasaccharide, the  $\text{Man}_6\text{-}\alpha 1 \rightarrow 6\text{-Man}_m$  fragment also plays a very important role in determining the overall shape of the Asn-linked oligosaccharides. Unlike other linkages, the two saccharides linked through  $\alpha 1 \rightarrow 6$ -linkage are separated by three bonds and naturally  $\alpha 1 \rightarrow 6$ -linked disaccharides have much more conformational flexibility associated with them. The third glycosidic torsion angle,  $\chi$ , could have either of the three staggered conformations ( $60^\circ$ ,  $-60^\circ$  and  $180^\circ$ ). Traditionally, while discussing the conformation of  $\text{Man-}\alpha 1 \rightarrow 6\text{-Man}$  fragments,  $\psi$  was assumed to be around  $180^\circ$  and the conformation with  $\chi$  around  $60^\circ$  has been considered less probable because of the Hassel-Ottar effect (unfavorable

syn-axial interactions between the O4 and O6 atoms [52]). For the  $\text{Man-}\alpha 1 \rightarrow 6\text{-Man}$  disaccharide, in all the 1000 ps MD simulations started with the three initial conformations  $\phi, \psi, \chi = -60^\circ, 150^\circ, 180^\circ$ ;  $-60^\circ, 150^\circ, -60^\circ$  and  $-60^\circ, 150^\circ, 60^\circ$  [38],  $\phi$  shows fluctuations from  $-60^\circ$  to  $60^\circ$  (through  $0^\circ$ ) and  $\psi$  shows fluctuations from  $60^\circ$  to  $-60^\circ$  (through  $180^\circ$ ). In contrast,  $\chi$  fluctuates around one of the three staggered conformations:  $60^\circ$ ,  $180^\circ$ , or  $-60^\circ$ . Although in the simulation started with  $\chi = 180^\circ$   $\chi$  did not show any transition from the initial value during the 1000 ps simulation period, the  $\chi$  shows transitions from one staggered conformation to another in the other two simulations. However, in a simulation which was run for 3000 ps (with initial  $\chi = 180^\circ$ ), though the fluctuations of  $\phi$  and  $\psi$  are very similar to those in the 1000 ps simulations,  $\chi$  moves from  $180^\circ$  to  $-60^\circ$  after about 1250 ps, and then from  $-60^\circ$  to  $60^\circ$  after about 2100 ps (Fig. 7). In the conformation where  $\chi$  is around  $60^\circ$  the 'repulsive' syn-axial interaction between O4 and O6 atoms is offset by a hydrogen bond interaction between the two atoms. In the absence of this hydrogen bond (i.e. if O4 forms a hydrogen bond with the solvent molecules), the conformation with  $\chi$  around  $60^\circ$  may become unfavorable.

In oligosaccharide simulations, unlike the disaccharide simulations, transition of  $\chi_6$  to around  $60^\circ$  was observed only in M3XF (where  $\text{Man}_6$  is the terminal residue [38]) and M9 [40]. In the simulations of M3G3G3 started with initial  $\chi_6 = 60^\circ$ ,  $\chi_6$  changes from around  $60^\circ$  to around  $180^\circ$  after about 920 ps [39]. In other oligosaccharides,  $\chi_6$  assumes conformations only around either  $180^\circ$  or  $-60^\circ$  [39,40]. In high

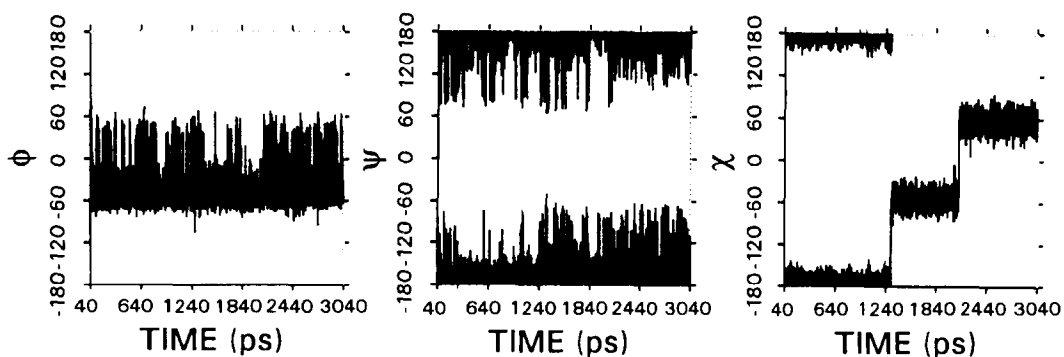


Fig. 7. Variation of the interglycosidic torsion angles  $\phi, \psi, \chi$  in the MD simulations of the disaccharide  $\text{Man-}\alpha 1 \rightarrow 6\text{-Man}$  (from Ref. [38]).

mannose and hybrid oligosaccharides, in contrast to  $\chi_6$ ,  $\chi_{66}$  shows transitions among all the three staggered conformations [40,41]. The  $\phi_6, \psi_6, \chi_6$  values are interdependent and in several simulations,  $\phi_6$  and  $\psi_6$  prefer values other than around  $-60^\circ$  and  $180^\circ$  respectively. High mannose (except M9) and hybrid oligosaccharides showed a preference for the conformation with  $\phi_6, \psi_6, \chi_6$  around  $-60^\circ, 180^\circ, -60^\circ$  and in this conformation, the Man<sub>36</sub>-O2 to GlcNAc<sub>2</sub>-O7 hydrogen bond is possible. Earlier NMR studies [53] had predicted that this hydrogen bond accounts for the preference of high mannose oligosaccharides for the conformations with  $\chi_6$  around  $-60^\circ$ . Man<sub>36</sub>-O2 in M6b, M7b, M7d, M8a and M8c, is further extended by the addition of Man<sub>236</sub>, preventing the formation of the hydrogen bond with GlcNAc<sub>2</sub>-O7. In these oligosaccharides also,  $\phi_6, \psi_6, \chi_6$  prefer values around  $-60^\circ, 180^\circ, -60^\circ$  indicating that the preference for this is independent of the aforementioned hydrogen bond alone [40].

### 5.3.1. Importance of the torsion angle $\psi$ of $\alpha 1 \rightarrow 6$ -linkages

As mentioned earlier, in the MD simulations of the disaccharide Man- $\alpha 1 \rightarrow 6$ -Man,  $\phi$  shows fluctuations from  $-60^\circ$  to  $60^\circ$  (through  $0^\circ$ ) and  $\psi$  shows fluctuations from  $60^\circ$  to  $-60^\circ$  (through  $180^\circ$ ; Fig. 7), but in oligosaccharides, the fluctuations of  $\phi_6$  and  $\psi_6$  around the  $\alpha 1 \rightarrow 6$ -linkage are restricted. In high mannose oligosaccharides (except M9),  $\psi_6$  prefers a value around  $180^\circ$ . In M9 and hybrid oligosaccharides,  $\psi_6$ , in addition to values around  $180^\circ$  also prefers values around  $-60^\circ$  to  $-150^\circ$  (correlated to  $\chi_6$ ). In some complex oligosaccharides,  $\psi_6$  seems to prefer values around  $180^\circ$  although values around  $70^\circ$  and  $-70^\circ$  are also accessed occasionally, as for example in M3G1 [41]. In others,  $\psi_6$  seems to prefer values around  $70^\circ$  and rarely accesses conformations around  $180^\circ$  (as in M3G2). This shows that the conformation around the  $\alpha 1 \rightarrow 6$ -linkage is influenced significantly by the addition/deletion of saccharides. This is also noteworthy since the orientation of the  $\alpha 1 \rightarrow 6$ -arm is not only affected by changes in  $\chi$ , but also by changes in  $\phi$  and  $\psi$ . This can be seen clearly by considering M3XF as an example: in Fig. 8, four conformers of M3XF that are accessed during the MD trajectory are shown keeping the middle mannose residue (Man<sub>m</sub>) in the same orientation. Comparison of Fig. 8(a) and

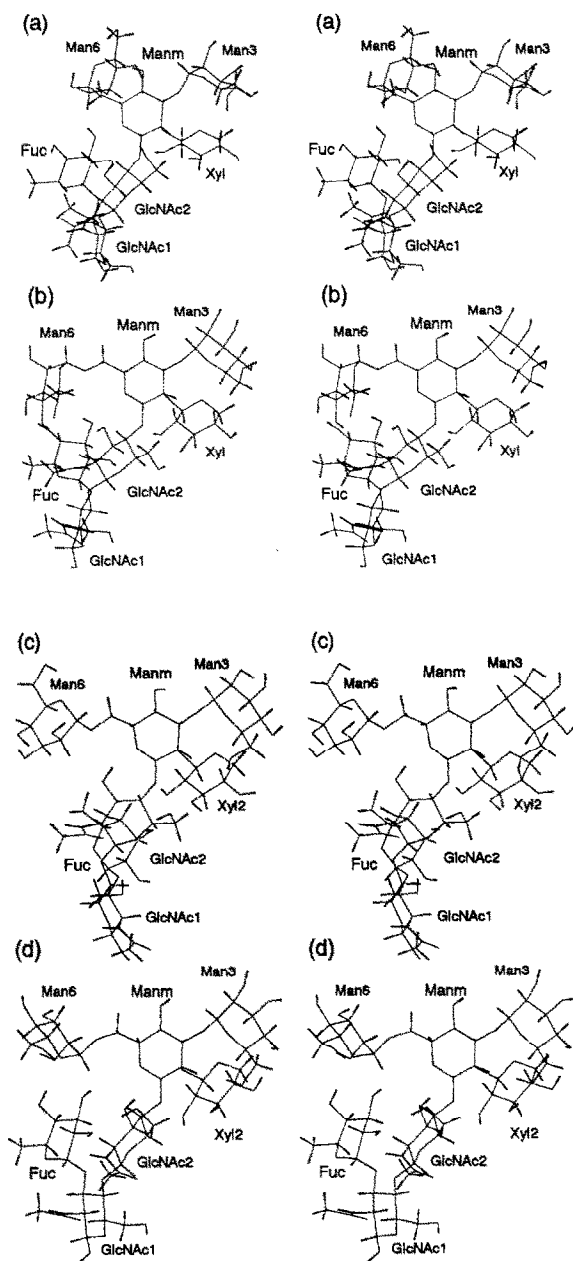


Fig. 8. Stereo view of the heptasaccharide M3XF showing the differences in the orientation of the  $\alpha 1 \rightarrow 6$ -arm brought about by the changes in  $\chi_6$  alone (a compared to b, c, d) and in  $\phi_6, \psi_6$  (b, c and d).  $\phi_6, \psi_6, \chi_6$  values are:  $-50^\circ, -161^\circ, -175^\circ$  (a);  $-60^\circ, -179^\circ, -58^\circ$  (b);  $-45^\circ, -106^\circ, -55^\circ$  (c); and  $-64^\circ, -110^\circ, -55^\circ$  (d). The four conformers were first superposed over one another using the C1, C3, C5 and O5 atoms of the middle mannose residue (Man<sub>m</sub>) for alignment, and then separated to eliminate spurious orientational differences. See legend to Fig. 5 for color codes used.

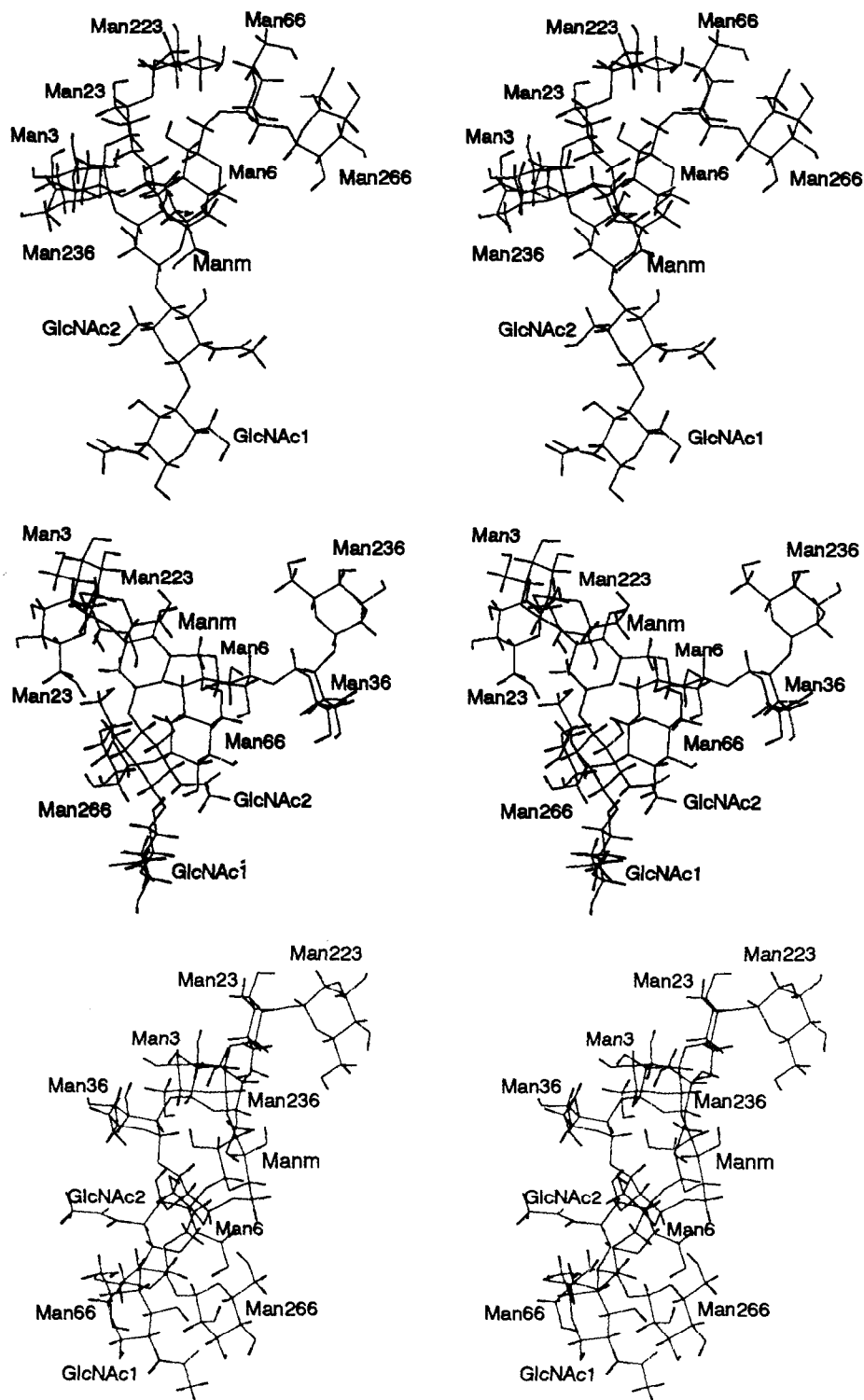


Fig. 9. Stereo diagram of the three conformers of M9 accessed during MD simulations.  $\phi_6, \psi_6, \chi_6$  are: (a)  $-42^\circ, -176^\circ, -173^\circ$  (top); (b)  $-22^\circ, -82^\circ, -13^\circ$  (middle); and (c)  $14^\circ, 81^\circ, 175^\circ$  (bottom) respectively. See legend to Fig. 5 for color codes used.

Fig. 8(b) shows the effect of change in  $\chi$  from around  $180^\circ$  to around  $-60^\circ$  ( $\phi$  and  $\psi$  being very nearly the same). In Fig. 8(b)–(d),  $\chi$  is around  $-60^\circ$  whereas  $\phi$  and  $\psi$  are different. Similar observations have also been made in the simulations of M9 (Fig. 9) and M3G2 [41].

#### 5.4. $\beta 1 \rightarrow 4$ -linkages

The MD simulations of the disaccharide GlcNAc- $\beta 1 \rightarrow 4$ -GlcNAc [38] showed that the interglycosidic torsion angles  $\phi, \psi$  access all the minimum energy conformations except  $70^\circ, -150^\circ$  and  $25^\circ, 175^\circ$  proposed from earlier molecular mechanics calculations [54,48]. The fluctuations of  $\phi, \psi$  in the disaccharide Man- $\beta 1 \rightarrow 4$ -GlcNAc, although very similar, are higher than those in GlcNAc- $\beta 1 \rightarrow 4$ -GlcNAc (Fig. 10(a) and (b); Ref. [38]). This is understandable since a change in the orientation of the hydroxyl group at C2 from equatorial (as in glucose) to axial (as in mannose), relieves some of the unfavorable steric contacts, and thereby increases the flexibility of the saccharide residues about the interglycosidic bonds [55]. However, when these two disaccharides are part of a larger oligosaccharide, as for example in the different types of Asn-linked oligosaccharides, the fluctuations of the corresponding torsion angles

$\phi_{g1}, \psi_{g1}$  and  $\phi_m, \psi_m$  (Fig. 3) are restricted and are mostly around  $55^\circ, 0^\circ$  with a deviation of  $\pm 30^\circ$  [39,40]. However,  $\phi_{g1}$  and  $\phi_m$  in these oligosaccharides also access values in the range of  $140^\circ$ – $165^\circ$ . In the hybrid oligosaccharides M5G1 and M5G2B (i.e. both bisected and unbisected), whenever  $\chi_6$  prefers a value around  $180^\circ$   $\phi_{g1}$  and  $\phi_m$  showed a preference for values around  $140^\circ$  to  $165^\circ$  [41]. The fluctuations of  $\phi_4, \psi_4$ , which determine the conformation of the bis-GlcNAc in bisected hybrid and complex oligosaccharides (GlcNAc $_4$ - $\beta 1 \rightarrow 4$ -Man $_m$  fragment), are restricted to values around  $55^\circ, 10^\circ$  as in the case of  $\phi_{g1}, \psi_{g1}$  and  $\phi_m, \psi_m$ , but transitions of  $\phi_4$  to the  $140^\circ$ – $165^\circ$  region was not observed in any of these simulations. This implies that bis-GlcNAc has rather limited flexibility and its relative orientation with respect to the middle mannose residue, Man $_m$ , remains very nearly the same. Similar conclusions about the restricted flexibility of  $\phi_4, \psi_4$  have also been drawn from NMR studies [51]. The conformation around the  $\beta 1 \rightarrow 4$ -linkage connecting Gal $_{443}$ - $\beta 1 \rightarrow 4$ -GlcNAc $_{43}$  fragment to Man $_3$  in M3G3G3 is similar to that for bis-GlcNAc, in that  $\phi_{43}, \psi_{43}$  fluctuate around  $55^\circ, 0^\circ$  and  $\phi_{43}$  does not show transitions to the  $140^\circ$ – $165^\circ$  region [39]. In contrast,  $\phi_{423}, \psi_{423}, \phi_{443}, \psi_{443}$  and  $\phi_{426}, \psi_{426}$ , which determine the conformations of the terminal galactose residues in the

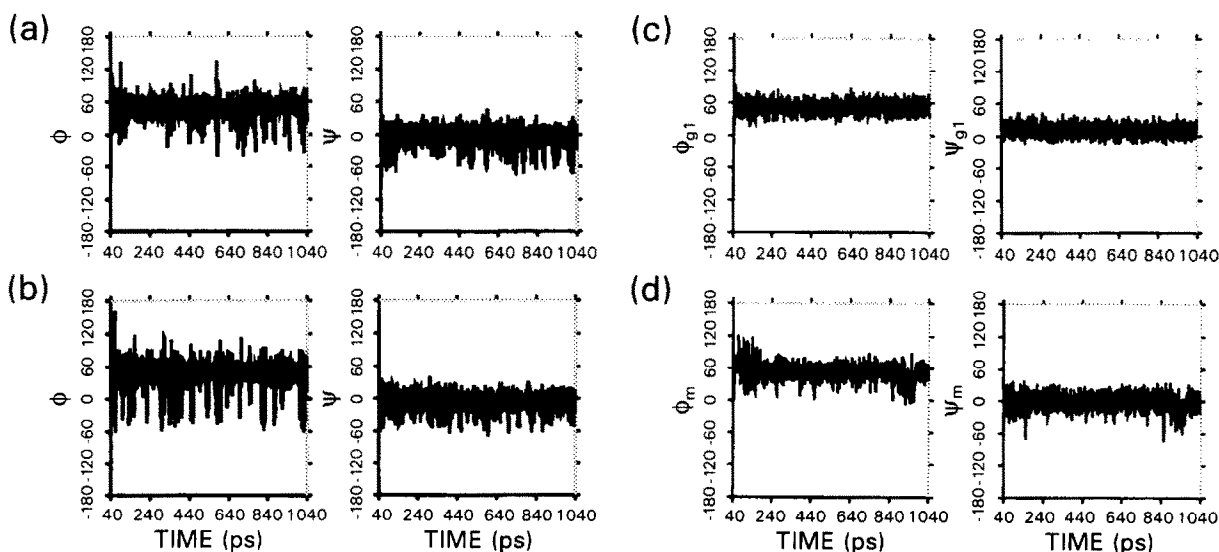


Fig. 10. Variation of the interglycosidic torsion angles of  $\beta 1 \rightarrow 4$ -linkages in the MD simulations of the disaccharides (a) GlcNAc- $\beta 1 \rightarrow 4$ -GlcNAc and (b) Man- $\beta 1 \rightarrow 4$ -GlcNAc and (c,d) the oligosaccharide M3XF.  $\phi, \psi$  in (a) and (b),  $\phi_{g1}, \psi_{g1}$  in (c), and  $\phi_m, \psi_m$  in (d).

complex oligosaccharide M3G3G3, show a lot of fluctuations and the terminal galactose residues often 'flip' relative to the penultimate GlcNAc residue because of  $\phi$  accessing values in the region  $140^\circ$ – $165^\circ$  [39]. The  $\phi, \psi$  values obtained in these simulations are in good agreement with those obtained by earlier force field calculations [46,47,49].

These MD simulations also provided some information on the effect of the other saccharide residues in the oligosaccharide on the conformational behavior of the core  $\beta 1 \rightarrow 4$ -linkages. For example, the fluctuations of  $\phi_{g1}, \psi_{g1}$  and  $\phi_m, \psi_m$  are very much dampened when GlcNAc<sub>1</sub> is  $\alpha 1 \rightarrow 3$ -fucosylated as in the oligosaccharide M3XF (Fig. 10(c) and (d)). This effect is probably caused by the spatial proximity of the  $\alpha 1 \rightarrow 3$ -linked fucose to GlcNAc<sub>1</sub>. The nature of saccharide

residues linked to Man<sub>6</sub> was also found to influence the favored values of  $\phi_m, \psi_m$ . In the absence of any substitution on Man<sub>6</sub> as in M3G1B, the fluctuations in  $\phi_{g1}, \psi_{g1}$  and  $\phi_m, \psi_m$  are very similar to those found in isolated disaccharides. However, in the simulations of high mannose, hybrid and complex oligosaccharides where one or more 'antennae' are linked to Man<sub>6</sub> the fluctuations in  $\phi_m, \psi_m$  are considerably less because of the spatial proximity of one of the 'antennae' to the core GlcNAc residues. Thus, the conformation of the Man<sub>m</sub>- $\beta 1 \rightarrow 4$ -GlcNAc<sub>2</sub>- $\beta 1 \rightarrow 4$ -GlcNAc<sub>1</sub> fragment is influenced by the conformation of the Man<sub>6</sub>- $\alpha 1 \rightarrow 6$ -Man<sub>m</sub> fragment. Contrarily, bis-GlcNAc does not seem to have any direct effect on the conformation of the core  $\beta 1 \rightarrow 4$ -linkages.

Hydrogen bonds between GlcNAc<sub>1</sub>-O3 and

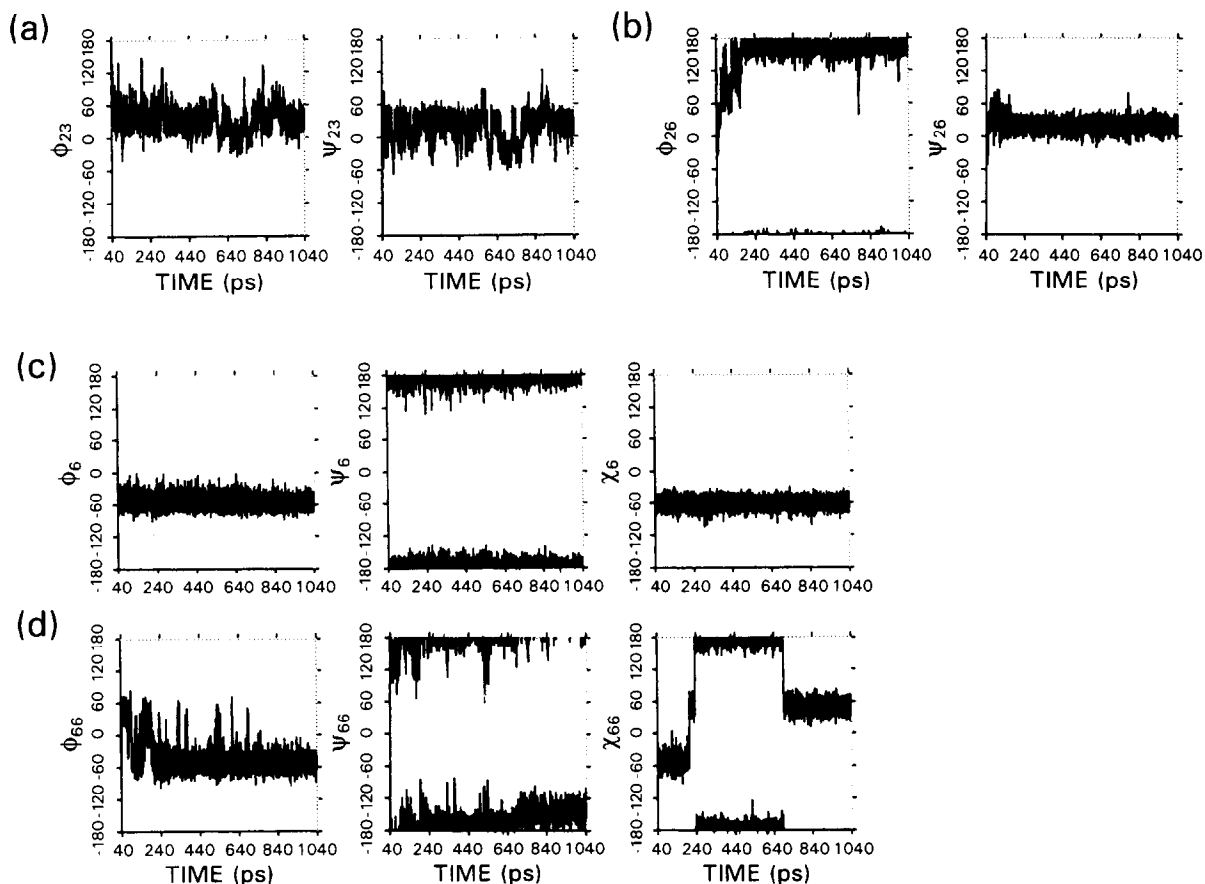


Fig. 11. Variation of the interglycosidic torsion angles around (a,b)  $\beta 1 \rightarrow 2$ - and (c,d)  $\alpha 1 \rightarrow 6$ -linkages. Torsion angle versus time plots for (a)  $\phi_{23}, \psi_{23}$  and (b)  $\phi_{26}, \psi_{26}$  extracted from the dynamics trajectories of M3G3G3 and for (c)  $\phi_6, \psi_6, \chi_6$  and (d)  $\phi_{66}, \psi_{66}, \chi_{66}$  from the MD trajectories of M8a (from Ref. [38]).

GlcNAc<sub>2</sub>-O5 and GlcNAc<sub>2</sub>-O3 and Man<sub>m</sub>-O5 are possible in both the di- and the oligosaccharides. Hydrogen bonds between GlcNAc<sub>1</sub>-O3 and GlcNAc<sub>2</sub>-O6 (GlcNAc<sub>2</sub>- $\chi = 180^\circ / -60^\circ$ ) and between GlcNAc<sub>1</sub>-O6 (GlcNAc<sub>2</sub>- $\chi = 60^\circ$ ) and GlcNAc<sub>2</sub>-O7, are also possible but the donor-acceptor distance shows large fluctuations (3–5 Å). However, all the above mentioned hydrogen bonds are broken when  $\phi$  takes a value around  $165^\circ$  in which case only a hydrogen bond between GlcNAc<sub>1</sub>-O3 and GlcNAc<sub>2</sub>-O7 is possible.

### 5.5. $\alpha 1 \rightarrow 2$ -linkages

Although all the  $\alpha 1 \rightarrow 2$ -linkages in high mannose type oligosaccharides favor a conformation around  $-40^\circ, 0^\circ$ , the extent of variation of these torsion angles is different in different oligomannose structures. For the Man<sub>23</sub>- $\alpha 1 \rightarrow 2$ -Man<sub>3</sub> fragment in M6a, M7b, M7c, and M8c,  $\psi_{23}$  fluctuates more ( $\pm 40^\circ$ ) than  $\phi_{23}$  ( $\pm 25^\circ$ ) [40]. However,  $\phi_{23}$  occasionally accesses conformations in the range  $0^\circ$  to  $60^\circ$  also. The conformations of the terminal  $\alpha 1 \rightarrow 2$ -linked mannoses

Man<sub>223</sub> and Man<sub>266</sub> are similar to Man<sub>23</sub>. In all the oligomannoses (except some conformations of M9), Man<sub>236</sub> is placed very close to core GlcNAc<sub>2</sub> which restricts its conformational fluctuations. The values of  $\phi, \psi$  obtained in these MD simulations for  $\alpha 1 \rightarrow 2$ -linkages are in good agreement with those obtained by earlier force field calculations [46,48,49,34]. A hydrogen bond between Man<sub>23</sub>-O6 (with Man<sub>23</sub>- $\chi$  around  $-60^\circ$ ) and Man<sub>3</sub>-O5 is possible when  $\psi_{23}$  is in the positive region (i.e. greater than  $0^\circ$ ). This hydrogen bond is also possible for the terminal mannose residues.

### 5.6. $\beta 1 \rightarrow 2$ -linkages

Conformational fluctuations of  $\phi$  and  $\psi$  for  $\beta 1 \rightarrow 2$ -linkages in both the hybrid and complex oligosaccharides are mostly between  $0^\circ$  and  $70^\circ$ , and  $-40^\circ$  and  $60^\circ$ , respectively. As in the case of  $\beta 1 \rightarrow 4$ -linkages,  $\phi$  in  $\beta 1 \rightarrow 2$ -linkages also frequently accesses values from  $140^\circ$  to  $180^\circ$  leading to the flipping of one saccharide relative to the other. In the bisected hybrid and complex oligosaccharides, the conformational fluctuations

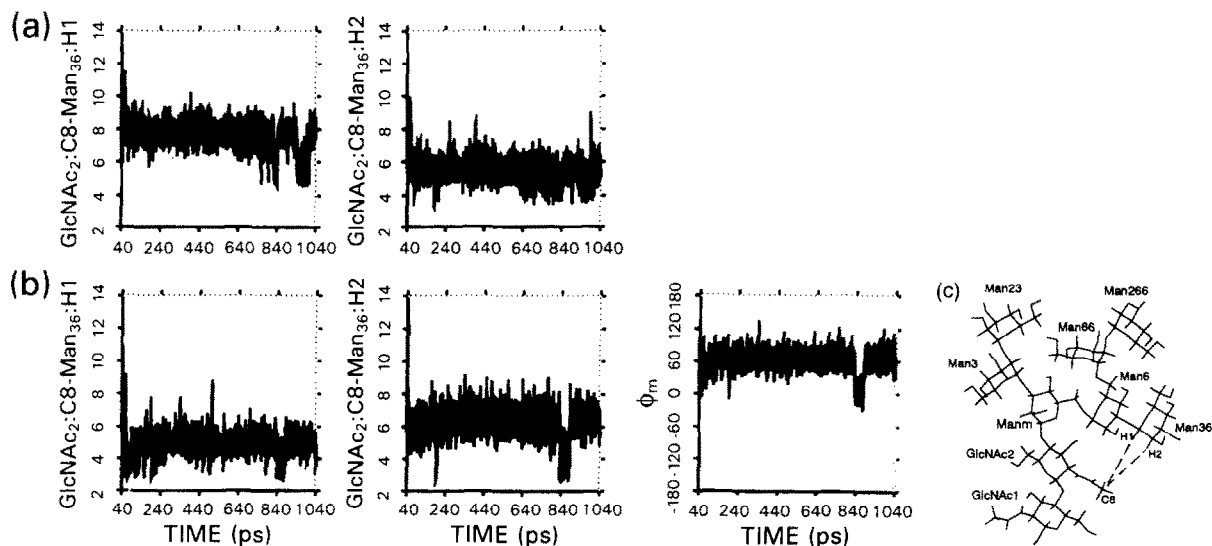


Fig. 12. Variation in the distance (Å) of the H1 (left panels) and H2 (middle panels) atoms of Man<sub>36</sub> from the C8 atom of GlcNAc<sub>2</sub> as a function of time extracted from the dynamics trajectories of (a) M8c and (b) M7c (MD data from Ref. [40]). As a result of the free rotation of the methyl group and the equivalence of the methyl protons in NMR, distances were calculated from the C8 atom instead of the protons attached to C8. Distances of the protons are assumed to be about 0.5 Å less than those from the C8 atom. Variation of the torsion angle  $\phi_m$  as a function of time in M7c is also shown (left panel). (c) Schematic diagram of M7c to show the C8, H1 and H2 atoms under discussion.

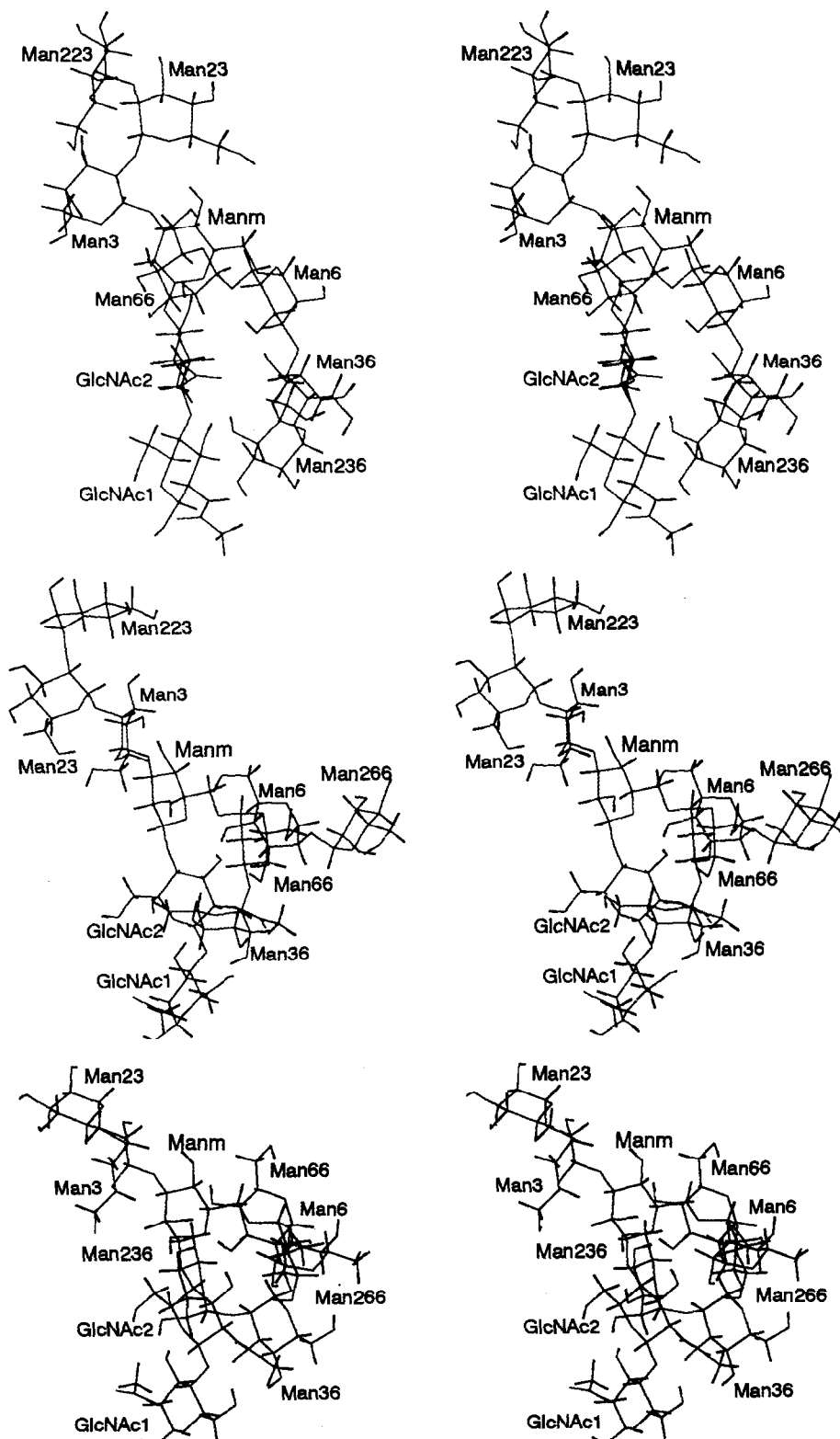
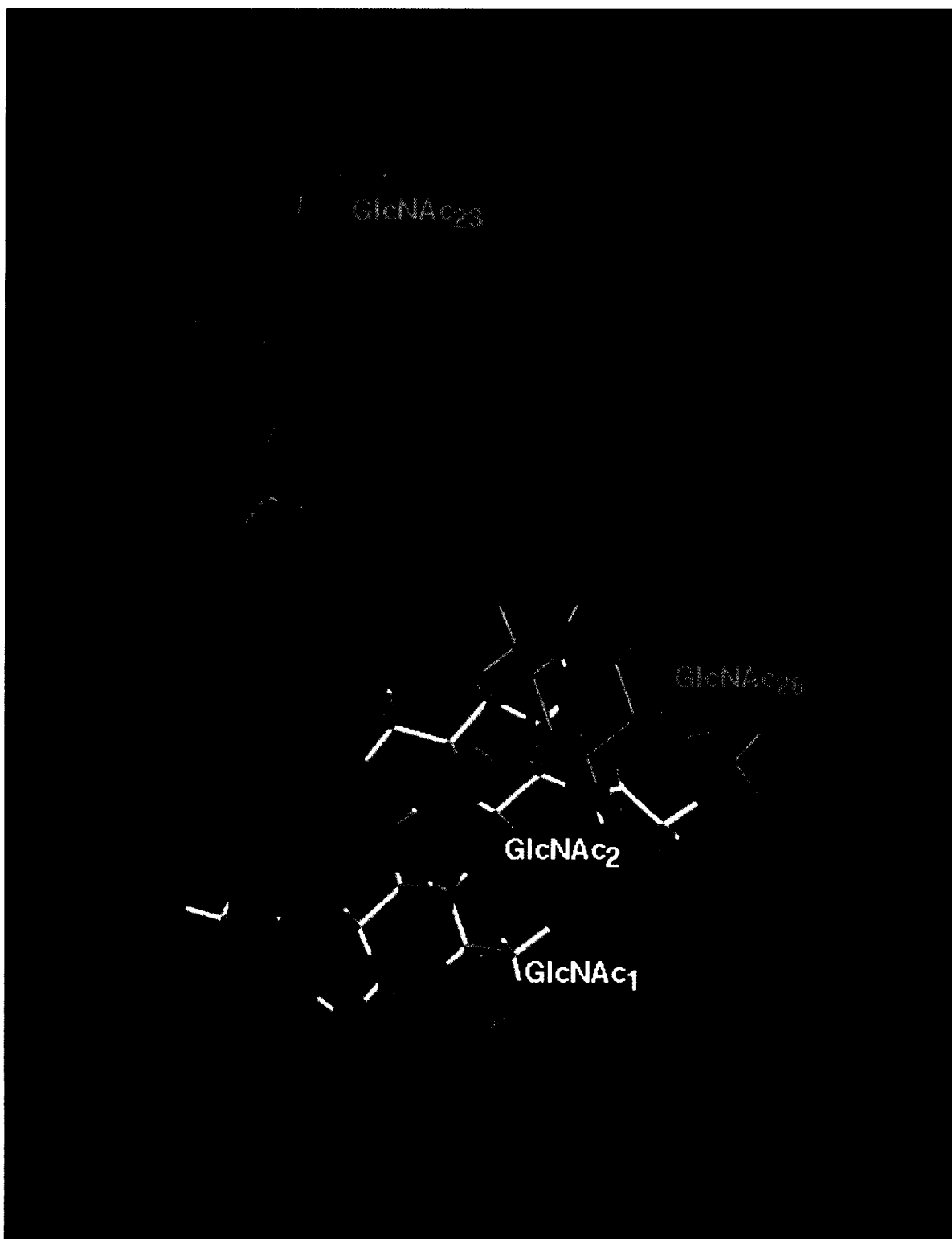


Fig. 13. Stereo diagram of the three isomers of  $\text{Man}_5\text{GlcNAc}_2$ . (a) M8a (top), (b) M8b (middle) and (c) M8c (bottom). The conformations are accessed in the MD trajectories at 742 ps, 196 ps, and 1034 ps, respectively (from Ref. [40]). See legend to Fig. 5 for color codes used.



of  $\phi_{23}, \psi_{23}$  are restricted because of the hydrophobic interaction between GlcNAc<sub>23</sub> and bis-GlcNAc as mentioned earlier. The average conformational angles obtained in these MD simulations for the  $\beta 1 \rightarrow 2$ -linkage are in good agreement with those reported from iso-energy contour maps of  $\beta 1 \rightarrow 2$ -linked disaccharides [42,56]. Conformation of Xyl- $\beta 1 \rightarrow 2$ -Man, either as an isolated disaccharide or as a part of a larger oligosaccharide, was found to be very similar to that of GlcNAc- $\beta 1 \rightarrow 2$ -Man fragment. In the GlcNAc- $\beta 1 \rightarrow 2$ -Man disaccharide fragment, hydrogen bond between Man-O3 and GlcNAc-O5 is possible when  $\phi$  is around  $60^\circ$ .

#### 5.6.1. Effect of $\chi_6$ on the conformation of GlcNAc<sub>26</sub>- $\beta 1 \rightarrow 2$ -Man<sub>6</sub> fragment

The conformational angles,  $\phi_{26}, \psi_{26}$  and  $\phi_{23}, \psi_{23}$ , for the GlcNAc- $\beta 1 \rightarrow 2$ -Man disaccharide fragments in M3G3G3 show a considerable amount of flexibility, and access conformations from  $-45^\circ$  to  $120^\circ$  ( $\phi$ ) and  $-60^\circ$  to  $120^\circ$  ( $\psi$ ) (Fig. 11(a)). However, the conformational angles  $\phi_{26}, \psi_{26}$  were found to correlate to  $\chi_6$ . Whenever  $\chi_6$  prefers a value around  $-60^\circ$ ,  $\phi_{26}$  changes from the  $60^\circ$  region to around  $165^\circ$  (Fig. 11(b)). In fact, in the crystal structure of the human Fc fragment and its complex with fragment B of protein A where  $\phi_{26}$  is close to  $180^\circ$   $\chi_6$  is around  $-60^\circ$  [29]. Thus, the two  $\beta 1 \rightarrow 2$ -linkages in the same oligosaccharide have different conformational preferences. Similar observations have also been made for the two  $\alpha 1 \rightarrow 3$ - (Fig. 4) and the two  $\alpha 1 \rightarrow 6$ -linkages (Fig. 11(c),(d)) in high mannose oligosaccharides [40], and the two inulobiose linkages in nystose [57]. This clearly shows that molecular models proposed for oligosaccharides based on the global minimum energy conformations of disaccharides need not necessarily lead to reliable results, and thus underlines the need for simulating the oligosaccharides by explicitly considering all the constituent saccharides.

## 6. Correlation of the experimental and MD simulations data

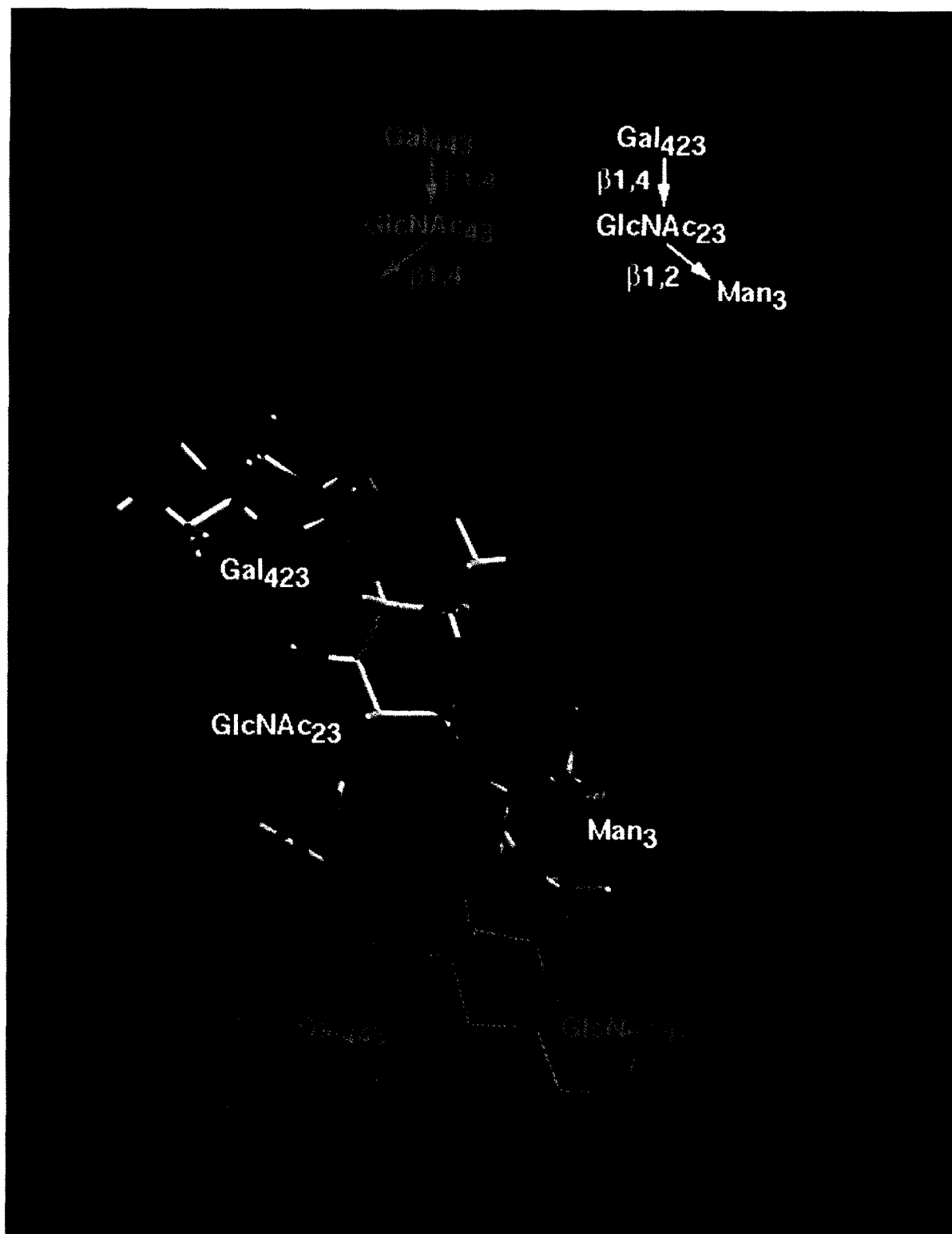
### 6.1. Effect of bis-GlcNAc on the Man<sub>3</sub>- $\alpha 1 \rightarrow 3$ -Man<sub>m</sub> fragment in complex oligosaccharides

From NOESY (Nuclear Overhauser Effect Spectroscopy) and ROESY (Rotating frame Overhauser Effect Spectroscopy) studies of M3G2 and M3G3B (Scheme 1), significant differences were found in the solution dynamic behavior of only the core  $\alpha 1 \rightarrow 3$ - and  $\alpha 1 \rightarrow 6$ -linkages [34,51]. In addition to differences in ROE intensities across Man<sub>3</sub>- $\alpha 1 \rightarrow 3$ -Man<sub>m</sub> in M3G2 and M3G3B, differences were also observed in the chemical shifts of Man<sub>m</sub>-H2 and Man<sub>m</sub>-H3. To account for these differences, it was suggested that the average location of Man<sub>3</sub>-O5 is proximal to Man<sub>m</sub>-H2 in M3G2, whereas Man<sub>3</sub>-O5 is farther from Man<sub>m</sub>-H2 but closer to Man<sub>m</sub>-H3 in M3G3B. In the light of these NMR studies, the distances of Man<sub>m</sub>-H2 and Man<sub>m</sub>-H3 from Man<sub>3</sub>-O5 were extracted from the MD trajectories of M3G2 and M3G3B [41]. The plots of distance as a function of time showed that the fluctuations in the distances are comparatively less in M3G3B than in M3G2. This is to be expected since as discussed earlier (Section 5.2), bis-GlcNAc has a dampening effect on the fluctuations of the Man<sub>3</sub>- $\alpha 1 \rightarrow 3$ -Man<sub>m</sub> fragment. However, as suggested from NMR studies, Man<sub>3</sub>-O5 atom is indeed closer to Man<sub>m</sub>-H3 than Man<sub>m</sub>-H2 in M3G3B. In M3G2, because of the large fluctuations in the distance between Man<sub>3</sub>:O5 and Man<sub>m</sub>:H2, Man<sub>3</sub>:O5 very frequently comes as close as 2.5 Å to Man<sub>m</sub>:H2. Thus the MD simulations data show qualitative agreement with the data from NMR studies.

#### 6.1.1. Orientation of Man<sub>36</sub> relative to GlcNAc<sub>2</sub> in M7c and M8c

The NMR studies on an intact glycoprotein, 13.6 kDa adhesion domain of human CD2, has also been reported recently [58]. This protein has a single

Fig. 14. One of the conformations accessed during the MD simulations of M3G2 (at 493 ps). Molecular graphic image was generated using MidasPlus. Color codes used for the GlcNAc residues of the core chitobiose, white; trimannosidic core mannoses, green; GlcNAcs attached to trimannosidic core (GlcNAc<sub>23</sub> and GlcNAc<sub>26</sub>), yellow. Oxygen and nitrogen atoms are colored red and blue respectively in all the saccharides.



glycosylation site at Asn65 and from NMR and electrospray ionization mass spectroscopy, the composition of the heterogenous *N*-glycan was determined to be 6% of M8c, 40% of M7c, and 34% of M6a (20% of Man<sub>5</sub> glycomers of unknown composition). Comparison of the NMR data of the oligosaccharides on glycoprotein with those from free model oligosaccharides showed significant differences only in the resonances of the core chitobiose GlcNAc residues. In addition, all the protein-oligosaccharide NOEs were assigned to the core GlcNAc residues, indicating that the saccharides beyond the middle mannose (Man<sub>m</sub>) are away from the protein and their conformation is similar to those in the free oligosaccharides. In view of this, data from the MD simulations of free M8c, M7c and M6a [40] were compared with those reported from the NMR studies [58] and were found to be consistent as discussed below.

The NMR data indicated that one arm of the glycan is folded towards the Man<sub>m</sub>-β1 → 4-GlcNAc<sub>2</sub>-β1 → 4-GlcNAc<sub>1</sub> fragment of the core, and such a folding of the α1 → 6-arm towards the core was also observed in the MD simulations. Among the many intra-oligosaccharide NOEs that were unambiguously assigned from the NMR study, two NOEs are from the Man<sub>36</sub>-H1 and Man<sub>36</sub>-H2 atoms with the GlcNAc<sub>2</sub> acetyl group (see Fig. 3(b) for atom nomenclature). Interestingly, these NOEs were observed in M7c (wherein Man<sub>36</sub> is the terminal residue; Scheme 1) but not in M8c (wherein Man<sub>236</sub> is linked to Man<sub>36</sub>). In view of this NOE data, distances of the Man<sub>36</sub>-H1 and Man<sub>36</sub>-H2 atoms from the GlcNAc<sub>2</sub>-C8 atom were extracted from the dynamics trajectories of M7c and M8c (Fig. 12). In M8c, the two protons of Man<sub>36</sub> are more than 5 Å away from the methyl group of GlcNAc<sub>2</sub> (Fig. 12(a)), which explains the absence of NOE between these atom pairs. However, in M7c, Man<sub>36</sub>-H1 is closer than 5 Å from GlcNAc<sub>2</sub>-C8 throughout the 1000 ps simulation period, but Man<sub>36</sub>-H2 is closer than 5 Å from GlcNAc<sub>2</sub>-C8 only

during 832 ps to 883 ps interval (Fig. 12(b)). These results suggest that the conformation accessed by M7c during the 832 ps to 883 ps interval corresponds to its conformation when it is part of a glycoprotein. The interglycosidic torsion angles which affect the distance between the atoms of GlcNAc<sub>2</sub> and Man<sub>36</sub> are  $\phi_m, \psi_m$  (Man<sub>m</sub>-β1 → 4-GlcNAc<sub>2</sub>),  $\phi_6, \psi_6, \chi_6$  (Man<sub>6</sub>-α1 → 6-Man<sub>m</sub>), and  $\phi_{36}, \psi_{36}$  (Man<sub>36</sub>-α1 → 3-Man<sub>6</sub>; Fig. 12(c)). Of these, only  $\phi_m$  changes from around 60° to around 0° between 832 ps to 883 ps (Fig. 12) suggesting that when M7c is part of the glycoprotein,  $\phi_m$  prefers a value around 0°.

Comparison of the conformations of M7c and M8c showed that the absence of the aforementioned NOEs in M8c is caused by the change in the conformation of Man<sub>36</sub>-α1 → 3-Man<sub>6</sub> fragment ( $\phi_{36}, \psi_{36}$  around -60°–30° in M7c and around 30°, 30° in M8c; Fig. 4; Section 5.2). The conformation of the Man<sub>6</sub>-α1 → 6-Man<sub>m</sub>-β1 → 4-GlcNAc<sub>2</sub> fragment was found to be essentially the same in both M7c and M8c ( $\phi_6, \psi_6, \chi_6$  around -60°, 180°, -60° and  $\phi_m, \psi_m$  around -60°, 0°). These data show that the conformation of an oligosaccharide will be affected by the addition or deletion of saccharides.

## 6.2. Occurrence of several mannosidases in ER and Golgi

Although several α1 → 2-mannosidases with different subcellular localization, molecular and biochemical properties have been characterized so far, as yet no information is available on the size of the oligosaccharide binding site of these enzymes [59,23,60]. The present simulations show that the relative orientation of each of the four Man-α1 → 2-Man disaccharide fragments is different with respect to the previous residue(s) (Fig. 9 and Fig. 13). If the binding site of these α1 → 2-mannosidases accommodates more than the Man-α1 → 2-Man disaccharide fragment (i.e. if they have extended binding sites), it is likely that some of the α1 → 2-mannosidases may be

Fig. 15. Pentasaccharide Gal<sub>443</sub>-β1 → 4-GlcNAc<sub>43</sub>-β1 → 4(Gal<sub>423</sub>-β1 → 4-GlcNAc<sub>23</sub>-β1 → 2)-Man<sub>3</sub> superposed over Gal<sub>463</sub>-β1 → 4-GlcNAc<sub>63</sub>-β1 → 6(Gal<sub>423</sub>-β1 → 4-GlcNAc<sub>23</sub>-β1 → 2)-Man<sub>3</sub>. Gal<sub>423</sub>-β1 → 4-GlcNAc<sub>23</sub>-β1 → 2-Man<sub>3</sub> fragment (green and white) which is common to both the pentasaccharides was taken as the reference point for superposition (C2 and O5 atoms of Gal<sub>423</sub>, C1 and C4 atoms of GlcNAc<sub>23</sub> and C2 and C5 atoms of Man<sub>3</sub>). The distance between the terminal galactose residues in both the pentasaccharides is about 15 Å. Molecular graphic images were generated using MidasPlus. Color codes used: Gal<sub>443</sub>-β1 → 4-GlcNAc<sub>43</sub>-β1 → , yellow; Gal<sub>463</sub>-β1 → 4-GlcNAc<sub>63</sub>-β1 → , cyan.

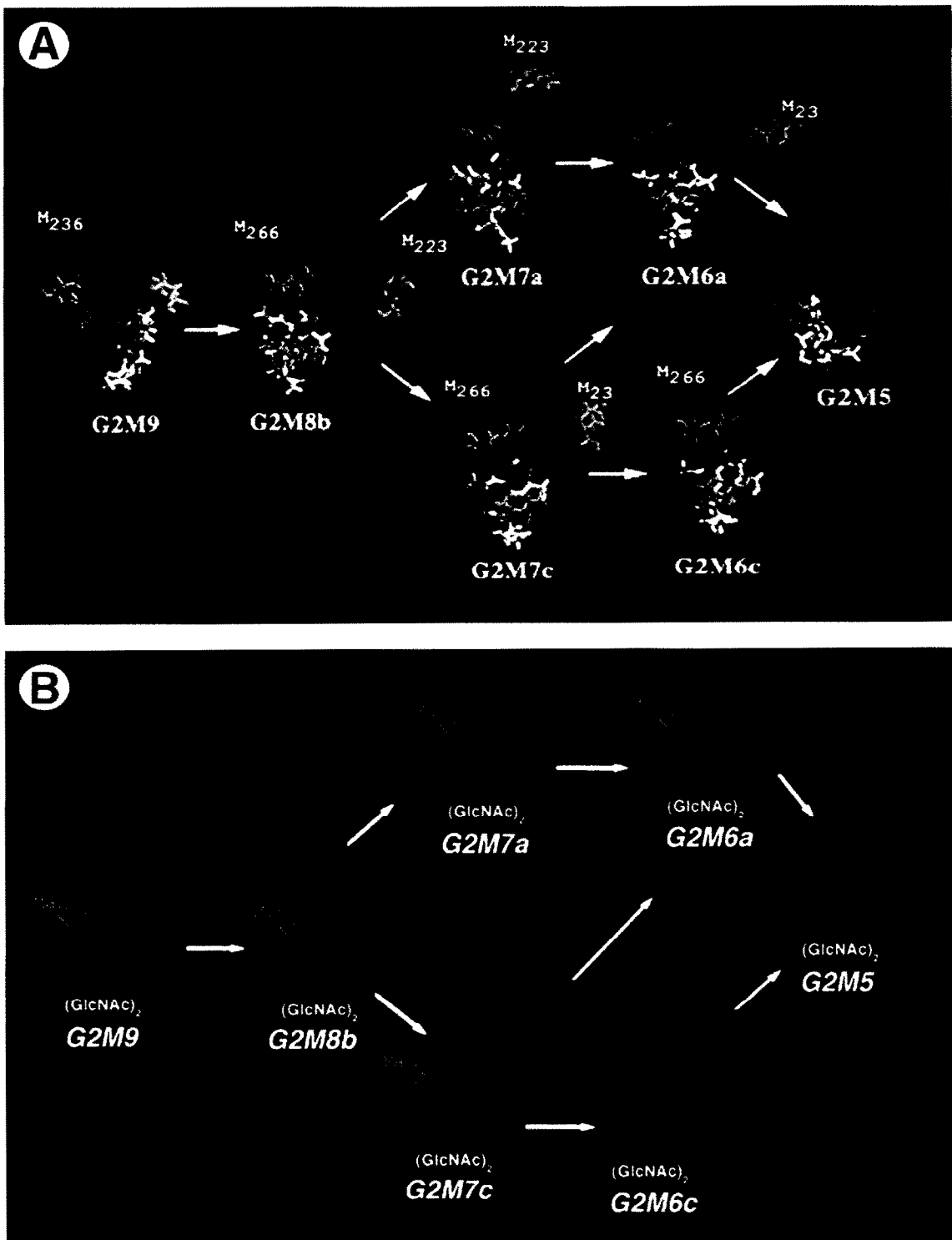


Fig. 16. I & II. Proposed pathways possible for the processing of M9 to M5 (from Ref. [40]).

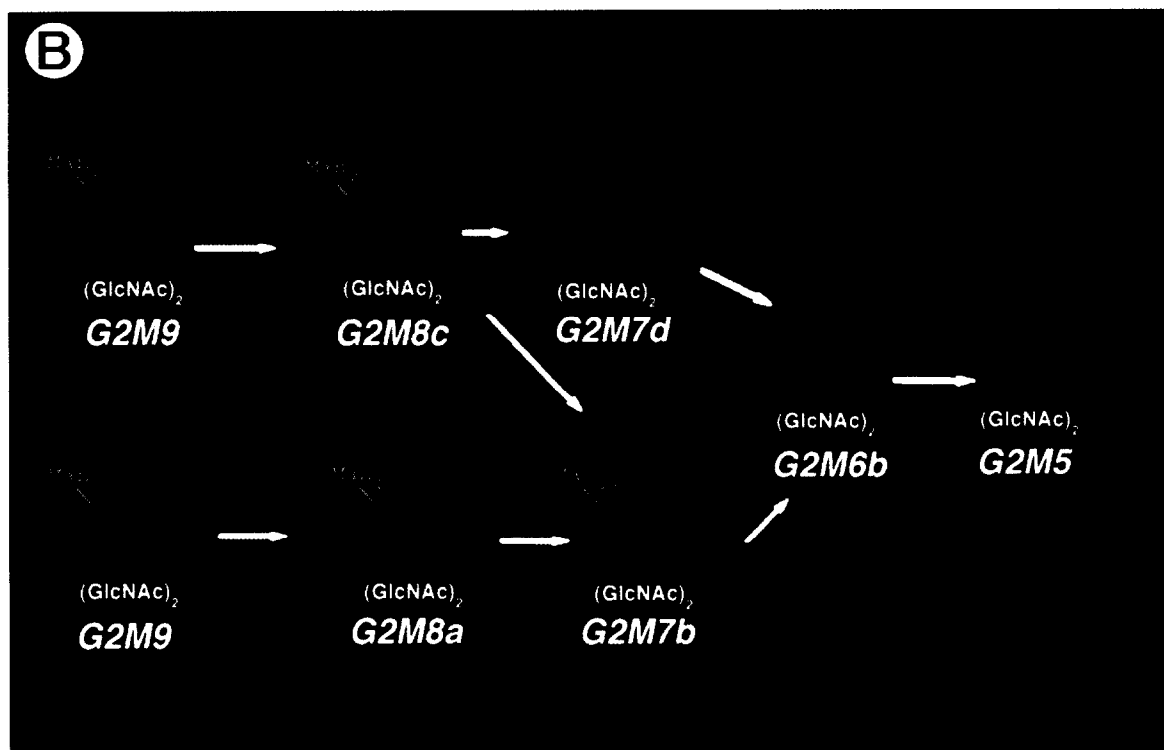
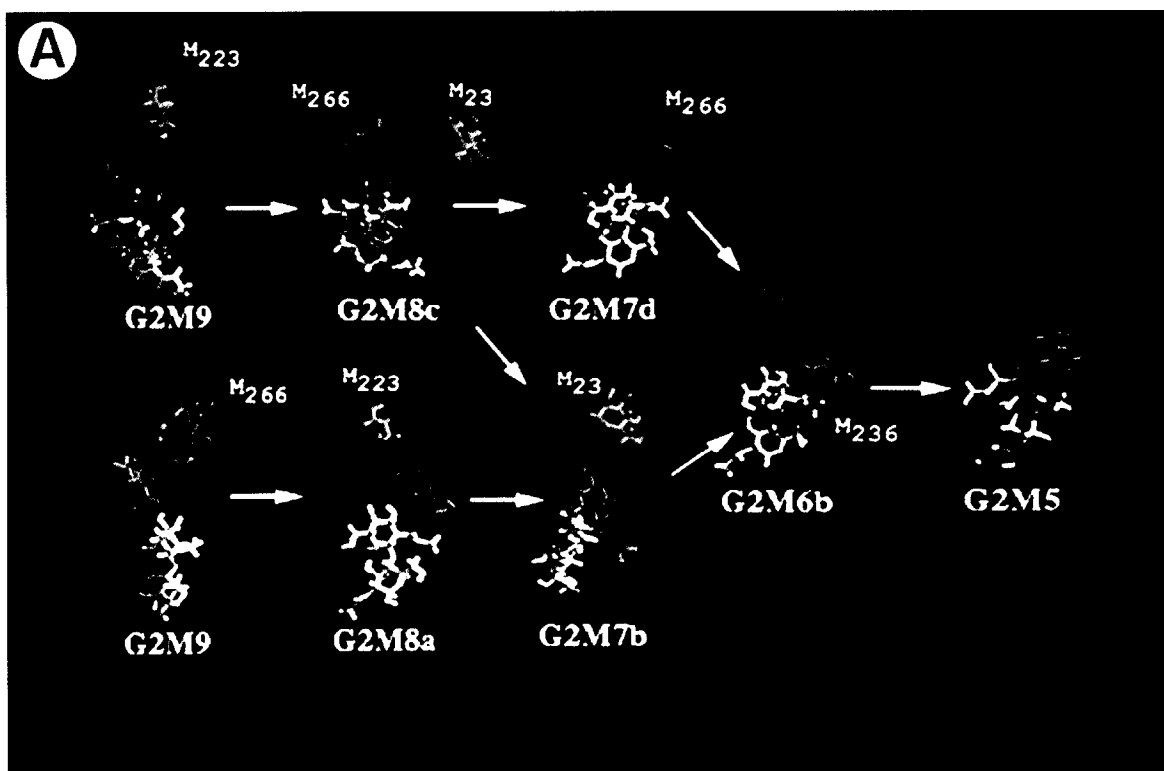


Fig. 16. Continued.

highly specific to the terminal mannose residues on certain arms/ branches. This perhaps explains the difference in the specificities of  $\alpha 1 \rightarrow 2$ -specific mannosidases present in the Golgi and ER. At least two ER  $\alpha$ -mannosidases are known, both of which act on M9 but produce different M8 isomers—one  $\alpha$ -mannosidase, which is inhibited by kifunensine, removes Man<sub>236</sub> of M9 to give M8b, whereas the other  $\alpha$ -mannosidase, which is not inhibited by kifunensine, removes Man<sub>266</sub> of M9 to give M8c [9].

### 6.2.1. Rate of cleavage of Man<sub>236</sub>

The MD simulations of high mannose type oligosaccharides have shown that the terminal  $\alpha 1 \rightarrow 2$ -linked mannose Man<sub>236</sub> is placed away from the core chitobiose residues in only some conformations of M9 (Fig. 9(b); Ref. [40]). The Man<sub>236</sub> residue in other conformations of M9 (Fig. 9(a), (c)), and in M8a (Fig. 13(a)), M8c (Fig. 13(c)), M7b, M7d and M6b, is placed very close to the core chitobiose mainly because of the preferred conformations of  $\phi_6, \psi_6, \chi_6$  around  $-60^\circ, 180^\circ, -60^\circ$ . Thus, if Man<sub>236</sub> is not cleaved from G2M9 in the first step, it will be cleaved only after the other three  $\alpha 1 \rightarrow 2$ -linked mannose residues are removed. Since in the preferred conformation of M6b, Man<sub>236</sub> is placed close to the chitobiose core, its accessibility to the solvent and hence to mannosidases is reduced. This may explain the 40-fold slower rate of cleavage of Man<sub>236</sub> as compared with other  $\alpha 1 \rightarrow 2$ -linked mannoses by ER Man<sub>9</sub>-mannosidase [61,62]. These authors also observed that the removal of the GlcNAc<sub>1</sub> residue of the chitobiose increased the hydrolytic susceptibility of the Man<sub>236</sub>- $\alpha 1 \rightarrow 2$ -Man<sub>36</sub> linkage. This further supports the conclusion drawn from the MD simulations that the slow rate of cleavage of Man<sub>236</sub> is caused by its close proximity to the core GlcNAc residues.

### 6.2.2. Addition of GlcNAc<sub>23</sub> by GlcNAc transferase I

It has been shown that the addition of GlcNAc<sub>23</sub> to Man<sub>3</sub> of M5 by GlcNAc transferase I is a necessary step in the biosynthesis of hybrid and complex type oligosaccharides. The MD simulations of M5 showed that  $\phi_6, \psi_6, \chi_6$  prefer a conformation around  $-60^\circ, 180^\circ, -60^\circ$  and cause Man<sub>36</sub> and Man<sub>66</sub> to be in close proximity to the core chitobiose. Thus, of the two  $\alpha 1 \rightarrow 3$ -linked mannose residues Man<sub>3</sub> and

Man<sub>36</sub>, Man<sub>3</sub> shows more flexibility than Man<sub>36</sub>, and is more exposed to the solvent (Fig. 5). This explains the preference of mannosidases to cleave Man<sub>3</sub> prior to Man<sub>36</sub> [63–65]. Hence, the addition of  $\beta 1 \rightarrow 2$ -linked GlcNAc to Man<sub>3</sub> by GlcNAc transferase I, in addition to being a prerequisite for mannosidase II action [66,67], may also reduce the accessibility of Man<sub>3</sub> to mannosidases.

### 6.2.3. Rate of addition of galactose to biantennary oligosaccharide M3G2

The MD simulations of the biantennary complex oligosaccharide M3G2 show that the fluctuations in  $\phi_{g1}, \psi_{g1}, \phi_m, \psi_m$  and  $\phi_6, \psi_6, \chi_6$  are restricted to a narrow region. In these conformations, of the two GlcNAc residues, GlcNAc<sub>26</sub> on the  $\alpha 1 \rightarrow 6$ -arm is close to the core chitobiose, whereas GlcNAc<sub>23</sub> on the  $\alpha 1 \rightarrow 3$ -arm is away from the core chitobiose and is more exposed (Fig. 14). This perhaps explains why the rate of addition of galactose to GlcNAc<sub>23</sub> by  $\beta 1 \rightarrow 4$ -galactosyltransferase is much faster than the rate of addition to GlcNAc<sub>26</sub> [68].

### 6.3. Differences in the binding affinities of two pentasaccharides to asialoglycoprotein receptor

Asialoglycoprotein receptor (ASGP-R) is present on the sinusoidal (blood-facing) surface of hepatocyte plasma membranes and binds terminal galactose or N-acetylgalactosamine residues of glycoproteins circulating in blood. This binding triggers the endocytosis of the receptor-bound asialoglycoprotein resulting in the clearance of the glycoprotein from blood circulation [69]. Ligand binding studies showed that the affinity of the ligands to ASGP-R increases exponentially with the number of terminal galactose residues (up to three residues [70]). Lee and coworkers [71] proposed a 'golden triangle' model to explain the binding of oligosaccharides according to which the three galactose binding sites of ASGP-R form the vertices of a golden triangle, and thus requires that the three terminal galactose residues to be in a precise geometric arrangement. However, two pentasaccharides—Gal<sub>463</sub>- $\beta 1 \rightarrow 4$ -GlcNAc<sub>63</sub>- $\beta 1 \rightarrow 4$ (Gal<sub>423</sub>- $\beta 1 \rightarrow 4$ -GlcNAc<sub>23</sub>  $\rightarrow 2$ )-Man<sub>3</sub> and Gal<sub>443</sub>- $\beta 1 \rightarrow 4$ -GlcNAc<sub>43</sub>- $\beta 1 \rightarrow 6$ (Gal<sub>423</sub>- $\beta 1 \rightarrow 4$ -GlcNAc<sub>23</sub>- $\beta 1 \rightarrow 2$ )-Man<sub>3</sub>—which are part of complex type of oligosaccharides and differ only in

one linkage ( $\beta 1 \rightarrow 4$  or  $\beta 1 \rightarrow 6$ ) showed about a 15-fold difference in their binding affinity to ASGP-R [70,72]. The MD simulations of these two pentasaccharides [39] showed that even though the distance between the two terminal galactose residues is very nearly the same in the two molecules, the relative orientation of the two galactose residues are different in the two pentasaccharides (Fig. 15), thereby explaining the differences in their binding affinities.

#### 6.4. Pathways for the processing of $\text{Man}_9\text{GlcNAc}_2$ to $\text{Man}_5\text{GlcNAc}_2$

Following the transfer of  $\text{Glc}_3\text{Man}_9\text{GlcNAc}_2$  precursor to the nascent polypeptide chain, glucosidase I and glucosidase II successively remove the  $\alpha 1 \rightarrow 2$ - and  $\alpha 1 \rightarrow 3$ -linked glucose residues forming  $\text{Man}_9\text{GlcNAc}_2$  or M9 oligosaccharide. This is further processed by  $\alpha 1 \rightarrow 2$ -linkage specific mannosidases to generate  $\text{Man}_5\text{GlcNAc}_2$  or M5 oligosaccharide. Several mannosidases have been identified both in the ER and Golgi, and have been shown to have different product specificities. It has been suggested that the processing of M9 to M5 proceeds in well defined 'conformation driven' sequential pathways [40]. Based on the conformations accessed by the high mannose type oligosaccharides in the MD simulations, possible pathways for the processing of M9 to M5 have been proposed (Fig. 16; from Ref. [40]). As mentioned earlier (Section 6.2), if  $\text{Man}_{236}$  of M9 is not cleaved first, it will be cleaved only after the other three  $\alpha 1 \rightarrow 2$ -linked mannoses have been cleaved. In one of the proposed pathways (Fig. 16(a)), M9 is converted to M8b by the ER  $\text{Man}_9$ -mannosidase which specifically hydrolyses the  $\alpha 1 \rightarrow 2$  linkage between  $\text{Man}_{236}$  and  $\text{Man}_{36}$  [19]. M5 can be generated from M8b either through M7a and M6a or through M7c and M6c. Part of this pathway involving the steps  $\text{M9} \rightarrow \text{M8b} \rightarrow \text{M7c/M7a} \rightarrow \text{M6a}$  is identical to the schemes proposed by Cohen and Ballou [20] from their nuclear magnetic resonance spectroscopic experiments, and by Tulsiani and Touster [73] by their studies on the action of rat liver mannosidase IA on M9. In the alternate pathway (Fig. 16(b)), M9 is converted to M8a by the second ER-resident  $\text{Man}_9$ -mannosidase [9], or to M8c (M8c can also be generated directly by the action of endomannosidase as

mentioned earlier; Section 2). Part of this pathway involving the steps  $\text{M9} \rightarrow \text{M8a} \rightarrow \text{M7b} \rightarrow \text{M6b}$  is identical to the scheme arrived at by Lee and coworkers [65] from their studies on the digestion of M9 by jack bean  $\alpha$ -mannosidase in vitro. It can be seen from the proposed pathways that there are no common intermediates between the two pathways. From this, and based on the observation that the ER-resident  $\text{Man}_9$ -mannosidases act only on certain M9 containing glycoproteins, it can be inferred that the initial conversion of M9 to M8 determines which of the high mannose oligosaccharides is likely to be present on the glycoproteins.

## 7. Conclusions

1. The MD simulations of several Asn-linked oligosaccharides have provided a wealth of information about their preferred and accessible conformations and have rationalized some of the biochemical and spectroscopic observations.
2. The conformational preferences of the interglycosidic torsion angles in the Asn-linked oligosaccharides are interdependent. Even those saccharide units which are distant in the primary sequence in the oligosaccharide, may affect the conformational preferences of a disaccharide fragment because of the spatial proximity in the oligosaccharide. Significant differences in the conformational preferences of interglycosidic torsion angles are also brought about by the addition/deletion of residues. Hence, the probable conformations of an oligosaccharide can not be derived from the conformational studies of its constituent di- and trisaccharides alone.
3. Asn-linked oligosaccharides are flexible molecules and the flexibility of the  $\alpha 1 \rightarrow 3$ - and the  $\alpha 1 \rightarrow 6$ -linkages in the common pentasaccharide core plays an important role in determining the overall 'shape' of the oligosaccharide compared to the flexibility associated with other linkages. Changes in the orientation of  $\alpha 1 \rightarrow 6$ -arm in the Asn-linked oligosaccharides are brought about not only by changes in  $\chi$  but also by changes in  $\phi$  and  $\psi$  for the same  $\chi$ .

4. Processing of Man<sub>9</sub>GlcNAc<sub>2</sub> to Man<sub>5</sub>GlcNAc<sub>2</sub> during the biosynthesis of Asn-linked oligosaccharides is 'conformation driven' and proceeds in a well-defined sequential manner. Possible pathways for this processing have been proposed, and certain segments of these proposed pathways are in agreement with those proposed based on earlier experimental studies. The preferred conformations of Man<sub>9</sub>GlcNAc<sub>2</sub> on the glycoprotein play an important role in setting the pathway for the processing steps.

### Acknowledgements

The authors acknowledge the National Cancer Institute for the allocation of computing time and staff support at the Frederick Biomedical Supercomputing Center of the Frederick Cancer Research and Development Center. Molecular graphics images were generated using the MidasPlus software system from the Computer Graphics Laboratory, University of California, San Francisco.

### References

- [1] K. Dill, E. Berman and A.A. Pavia, Natural abundance, <sup>13</sup>C-nuclear magnetic resonance spectral studies of carbohydrates linked to amino acids and proteins, *Adv. Carbohydr. Chem. Biochem.*, 43 (1985) 1–49.
- [2] E. Collier, J.-L. Carpentier, L. Beitz, H.P. Caro, S.I. Taylor and P. Gorden, Specific glycosylation site mutations of the insulin receptor  $\alpha$  subunit impair intracellular transport, *Biochemistry*, 32 (1993) 7818–7823.
- [3] S. Li, J. Schulman, S. Itamura and P. Palese, Glycosylation of neuraminidase determines the neurovirulence of influenza A/WSN/33 virus, *J. Virol.*, 67 (1993) 6667–6673.
- [4] D.J. Davidson and F.J. Castellino, The influence of the nature of the asparagine 289 linked oligosaccharide on the activation by urokinase and lysine binding properties of natural and recombinant human plasminogens, *J. Clin. Invest.*, 92 (1993) 249–254.
- [5] D.G. Fast, J.C. Jamieson and J. McCaffrey, The role of the carbohydrate chains of Gal- $\beta$ 1  $\rightarrow$  4-GlcNAc- $\alpha$ 2,6-Sialyltransferase for enzymatic activity, *Biochim. Biophys. Acta*, 1202 (1993) 325–340.
- [6] P.T. Richardson, K. Hussain, H.R. Woodland, J.M. Lord and L.M. Roberts, The effects of *N*-glycosylation on the lectin activity of recombinant ricin B chain, *Carbohydr. Res.*, 213 (1991) 19–25.
- [7] Y. Zhang and N.M. Dahms, Site directed removal of *N*-glycosylation sites in the bovine cation-dependent mannose 6-phosphate receptor — Effects on ligand binding, intracellular targeting and association with binding immunoglobulin protein, *Biochem. J.*, 295 (1993) 841–848.
- [8] R. Kornfeld and S. Kornfeld, Assembly of asparagine linked oligosaccharides, *Ann. Rev. Biochem.*, 54 (1985) 631–664.
- [9] S. Weng and R.G. Spiro, Demonstration that a kifunensine-resistant  $\alpha$ -mannosidase with a unique processing action on *N*-linked oligosaccharides occurs in rat liver endoplasmic reticulum and various cultured cells, *J. Biol. Chem.*, 268 (1993) 25 656–25 663.
- [10] W.A. Lubas and R.G. Spiro, Golgi endo- $\alpha$ -D-mannosidase from rat liver, a novel *N*-linked carbohydrate unit processing enzyme, *J. Biol. Chem.*, 262 (1987) 3775–3781.
- [11] A. Chapman, K. Fujimoto and S. Kornfeld, The primary glycosylation defect in class E Thy-1-negative mutant mouse lymphoma cells is an inability to synthesize dolichol phosphate mannose, *J. Biol. Chem.*, 255 (1980) 4441–4446.
- [12] K. Yamashita, J.P. Kamerling and A. Kobata, Structural study of the carbohydrate moiety of hen ovomucoid. Occurrence of a series of pentaantennary complex type asparagine linked sugar chains, *J. Biol. Chem.*, 258 (1983) 3099–3106.
- [13] A.J. Parodi, *N*-glycosylation in trypanosomatid protozoa, *Glycobiology*, 3 (1993) 193–199.
- [14] A.F. Williams, R.B. Parekh, D.R. Wing, A.C. Willis, A.N. Barclay, R. Dalchau, J.W. Fabre, R.A. Dwek and T.W. Rademacher, Comparative analysis of the *N*-glycans of rat, mouse and human Thy-1. Site-specific oligosaccharide patterns of neural Thy-1, a member of the immunoglobulin superfamily, *Glycobiology*, 3 (1993) 339–348.
- [15] S.E. Zamze, E.W. Wooten, D.A. Ashford, M.A.J. Ferguson, R.A. Dwek and T.W. Rademacher, Characterization of the asparagine-linked oligosaccharides from *Trypanosoma brucei* type-I variant surface glycoproteins, *Eur. J. Biochem.*, 187 (1990) 657–663.
- [16] N.M. Dahms and G.W. Hart, Mucence of quaternary structure on glycosylation: Differential subunit association affects the site-specific glycosylation of the common beta-chain from Mac-1 and LFA-1, *J. Biol. Chem.*, 261 (1986) 13 186–13 196.
- [17] E.D. Green and J.U. Baenziger, Asparagine-linked oligosaccharides on lutropin, follitropin, and thyrotropin. I. Structural elucidation of the sulfated and sialylated oligosaccharides on bovine, ovine, and human pituitary glycoprotein hormones, *J. Biol. Chem.*, 263 (1988) 25–35.
- [18] W.A. Lubas and R.G. Spiro, Evaluation of the role of rat liver Golgi endo- $\alpha$ -D-mannosidase in processing *N*-linked oligosaccharides, *J. Biol. Chem.*, 263 (1988) 3990–3998.
- [19] J. Bischoff, L. Liscum and R. Kornfeld, The use of 1-deoxymannojirimycin to evaluate the role of various  $\alpha$ -mannosidases in oligosaccharide processing in intact cells, *J. Biol. Chem.*, 261 (1986) 4766–4774.
- [20] R.E. Cohen and C.E. Ballou, Linkage and sequence analysis of mannose-rich glycoprotein core oligosaccharides by proton nuclear magnetic resonance spectroscopy, *Biochemistry*, 19 (1980) 4345–4358.
- [21] L. Moss, A. Prakobphol, T.-W. Wiedmann, S.J. Fisher and

- C. Damsky, Glycosylation of human trophoblast integrins is stage and cell-type specific, *Glycobiology*, 4 (1994) 567–575.
- [22] P. Hsieh, M.R. Rosner and P.W. Robbins, Selective cleavage by Endo- $\beta$ -*N*-acetylglucosaminidase H at individual glycosylation sites of sindbis virion envelope glycoproteins, *J. Biol. Chem.*, 258 (1983) 2555–2561.
- [23] K.W. Moremen, R.B. Trimble and A. Herscovics, Glycosidases of the asparagine-linked oligosaccharide processing pathway, *Glycobiology*, 4 (1994) 113–125.
- [24] M.D. Snider, Biosynthesis of glycoproteins: Formation of *N*-linked oligosaccharides, in V. Ginsburg and P.W. Robbins (eds.) *Biology of Carbohydrates*, John Wiley & Sons, New York, Vol. 2, 1984, pp. 163–198.
- [25] J.P. Carver and D.A. Cumming, Site-directed processing of *N*-linked oligosaccharides: The role of three-dimensional structure, *Pure Appl. Chem.*, 59 (1987) 1465–1476.
- [26] E.T. Baldwin, T.N. Bhat, S. Gulnik, M.V. Hosur, R.C. Sowder II, R.E. Cachau, J. Collins, A.M. Silva and J.W. Erickson, Crystal structures of native and inhibited forms of human cathepsin D: Implications for lysosomal targeting and drug design, *Proc. Natl. Acad. Sci. (USA)*, 90 (1993) 6796–6800.
- [27] Y. Bourne, P. Rouge and C. Cambillau, X-ray structure of a biantennary octasaccharide-lectin complex refined at 2.3 Å resolution, *J. Biol. Chem.*, 267 (1992) 197–203.
- [28] Y. Bourne, J. Mazurier, D. Legrand, R. Rouge, L. Montreuil, G. Spik and C. Cambillau, Structure of a legume lectin complexed with the human lactotransferrin N2 fragment, and with an isolated biantennary glycopeptide: Role of the fucose moiety, *Structure*, 2 (1994) 209–219.
- [29] J. Deisenhofer, Crystallographic refinement and atomic models of a human Fc fragment and its complex with fragment B of protein A from *Staphylococcus aureus* at 2.9 and 2.8 Å resolution, *Biochemistry*, 326 (1981) 358–363.
- [30] H.J. Hecht, H.M. Kalisz, J. Hendle, R.D. Schmid and D. Schomburg, Crystal structure of glucose oxidase from *Aspergillus niger* refined at 2.3 Å resolution, *J. Mol. Biol.*, 229 (1993) 153–172.
- [31] B. Shaanan, H. Lis and N. Sharon, Structure of a legume lectin with an ordered *N*-linked carbohydrate in complex with lactose, *Science*, 254 (1991) 862–866.
- [32] W.I. Weis, K. Drickamer and W.A. Hendrickson, Structure of a C-type mannose-binding protein complexed with an oligosaccharide, *Nature*, 360 (1992) 127–134.
- [33] D.A. Cumming and J.P. Carver, Virtual and solution conformation of oligosaccharides, *Biochemistry*, 26 (1987) 6664–6676.
- [34] S.W. Homans, A. Pastore, R.A. Dwek and T.W. Rademacher, Structure and dynamics in oligomannose type oligosaccharides, *Biochemistry*, 26 (1987) 6649–6655.
- [35] V.S.R. Rao, Protein–carbohydrate interactions—a theoretical approach, in P. Balaran and S. Ramaseshan, (eds.) *Molecular conformation and biological interactions*, Indian Academy of Sciences, Bangalore, 1991, pp. 411–427.
- [36] S.W. Homans, Conformation and dynamics of oligosaccharides in solution, *Glycobiology*, 3 (1993) 551–555.
- [37] A. Imberty and S. Perez, Molecular modeling of protein–carbohydrate interactions. Understanding the specificities of two legume lectins towards oligosaccharides, *Glycobiology*, 4 (1994) 351–366.
- [38] P.K. Qasba, P.V. Balaji and V.S.R. Rao, Molecular dynamics simulations of oligosaccharides and their conformation in the crystal structure of lectin–carbohydrate complex: Importance of the torsion angle  $\psi$  for the orientation of  $\alpha$ 1  $\rightarrow$  6-arm, *Glycobiology*, 4 (1994) 805–815.
- [39] P.V. Balaji, P.K. Qasba and V.S.R. Rao, Molecular dynamics simulations of asialoglycoprotein receptor ligands, *Biochemistry*, 32 (1993) 12599–12611.
- [40] P.V. Balaji, P.K. Qasba and V.S.R. Rao, Molecular dynamics simulations of highmannose oligosaccharides, *Glycobiology*, 4 (1994) 497–515.
- [41] P.V. Balaji, P.K. Qasba and V.S.R. Rao, Molecular dynamics simulations of hybrid and complex type Asn-linked oligosaccharides, *Int. J. Biol. Macromol.*, 18 (1996) 101–114.
- [42] B.K. Satyanarayana and V.S.R. Rao, Conformational studies of  $\beta$ -glucans, *Biopolymers*, 10 (1971) 1605–1615; erratum in *Biopolymers*, 11 (1971) 1115.
- [43] B.K. Satyanarayana and V.S.R. Rao, Conformational studies of  $\alpha$ -glucans, *Biopolymers*, 11 (1972) 1379–1394.
- [44] M. Biswas and V.S.R. Rao, Conformational studies on the ABH and Lewis blood group oligosaccharides, *Carbohydr. Polymers*, 2 (1982) 205–222.
- [45] M. Biswas, Y.C. Sekharudu and V.S.R. Rao, Conformational studies on some oligosaccharides related to N-glycosyl proteins which interact with Con A, *Int. J. Biol. Macromol.*, 8 (1986) 2–8.
- [46] M. Biswas, Y.C. Sekharudu and V.S.R. Rao, The conformation of glycans of the oligo-D-mannosidic type, and their interaction with Concanavalin A: A computer modeling study, *Carbohydr. Res.*, 160 (1987) 151–170.
- [47] S.W. Homans, A molecular mechanical force field for the conformational analysis of oligosaccharides: Comparison of theoretical and crystal structures of Man- $\alpha$ 1  $\rightarrow$  3-Man- $\beta$ 1  $\rightarrow$  4GlcNAc, *Biochemistry*, 29 (1990) 9110–9118.
- [48] A. Imberty, S. Gerber, V. Tran and S. Perez, Data bank of three dimensional structures of disaccharides. A tool to build three dimensional structures of oligosaccharides Part I. Oligomannose type N-glycans, *Glycoconjugate J.*, 7 (1990) 27–54.
- [49] T. Peters, B. Meyer, R. Stuike-Prill, R. Somorjai and J.-R. Brisson, A monte carlo method for conformational analysis of saccharides, *Carbohydr. Res.*, 238 (1993) 49–73.
- [50] T.E. Ferrin, C.C. Huang, L.E. Jarvis and L. Langridge, The MIDAS display system, *J. Mol. Graphics*, 6 (1988) 13–27.
- [51] T.J. Rutherford and S.W. Homans, Restrained and free molecular dynamics simulations of oligosaccharides: Application to solution dynamics of biantennary and bisected biantennary *N*-linked glycans, *Biochemistry*, 33 (1994) 9606–9614.
- [52] D. Hassel and B. Ottar, Lie structure of molecules containing cyclohexane or pyranose rings, *Acta Chem. Scand.*, 1 (1947) 929–942.
- [53] J.-R. Brisson and J.P. Carver, Solution conformation of asparagine linked oligosaccharides:  $\alpha$ (1–6)-linked moiety, *Biochemistry*, 22 (1983) 3680–3686.

- [54] M.R. Pincus, A.W. Burgess and H.A. Scheraga, Conformational energy calculations of enzyme-substrate complexes of lysozyme. I. Energy minimization of monosaccharide and oligosaccharide inhibitors and substrates of lysozyme, *Biopolymers*, 15 (1976) 2485–2521.
- [55] P.R. Sundararajan and V.S.R. Rao, Conformational studies of linear  $\beta$ -D-1  $\rightarrow$  4-mannan and galactan, *Biopolymers*, 9 (1970) 1239–1247.
- [56] A. Imberty, M.-M. Delage, Y. Bourne, C. Cambillau and S. Perez, Data bank of three dimensional structures of disaccharides: Part II, *N*-acetylglucosaminic type *N*-glycans. Comparison with the crystal structure of a biantennary octasaccharide, *Glycoconjugate J.*, 8 (1991) 456–483.
- [57] G.A. Jeffrey and D.-B. Huang, The tetrasaccharide nystose trihydrate: Crystal structure analysis and hydrogen bonding, *Carbohydr. Res.*, 247 (1993) 37–50.
- [58] D.F. Wyss, J.S. Choi and G. Wagner, Composition and sequence specific resonance assignments of the heterogenous *N*-linked glycan in the 13.6 kDa adhesion domain of human CD2 as determined by NMR on the intact glycoprotein, *Biochemistry*, 34 (1995) 1622–1634.
- [59] P.F. Daniel, B. Winchester and C.D. Warren, Mammalian  $\alpha$ -mannosidases—multiple forms but a common purpose? *Glycobiology*, 4 (1994) 551–566.
- [60] J.X. Ren, R.K. Brethauer and F.J. Castellino, Purification and properties of a Golgi-derived ( $\alpha$ 1  $\rightarrow$  2)-mannosidase I from baculovirus-infected lepidopteran insect cells (IPLB-SF21AE) with preferential activity toward mannose<sub>6</sub>-*N*-acetylglucosamine<sub>2</sub>, *Biochemistry*, 34 (1995) 2489–2495.
- [61] J. Schweden, G. Legler and E. Bause, Purification and characterization of a neutral processing mannosidase from calf liver acting on Man<sub>9</sub>GlcNAc<sub>2</sub> oligosaccharides, *Eur. J. Biochem.*, 157 (1986) 563–570.
- [62] E. Bause, W. Breuer, J. Schweden, R. Roeser and R. Geyer, Effect of substrate structure on the activity of Man<sub>9</sub>-mannosidase from pig liver involved in *N*-linked oligosaccharide processing, *Eur. J. Biochem.*, 208 (1992) 451–457.
- [63] E. Berman and A. Allerhand, Kinetics of  $\alpha$ -mannosidase action on various  $\alpha$ -D-mannopyranosyl linkages in hen ovalbumin glycopeptides as monitored by carbon 13 nuclear magnetic spectroscopy, *J. Biol. Chem.*, 256 (1981) 6657–6662.
- [64] F. Maley and R.B. Trimble, Revision of the structure for an endo- $\beta$ -*N*-acetylglucosaminidase H substrate using a novel modification of the Smith degradation, *J. Biol. Chem.*, 256 (1981) 1088–1090.
- [65] N. Tomiya, Y.C. Lee, T. Yoshida, Y. Wada, L. Awaya, M. Kurono and N. Takahashi, Calculated two-dimensional sugar map of pyridylaminated oligosaccharides: Elucidation of the jack bean  $\alpha$ -mannosidase digestion pathway of Man<sub>9</sub>GlcNAc<sub>2</sub>, *Anal. Biochem.*, 193 (1991) 90–100.
- [66] I. Tabas and S. Kornfeld, The synthesis of complex type oligosaccharides III. Identification of an  $\alpha$ -D-mannosidase activity involved in a late stage processing of complex type oligosaccharides, *J. Biol. Chem.*, 253 (1978) 7779–7786.
- [67] I. Tabas, S. Schlesinger and S. Kornfeld, Processing of high mannose oligosaccharides to form complex type oligosaccharides on the newly synthesized polypeptides of the vesicular stomatitis virus G protein and the IgG heavy chain, *J. Biol. Chem.*, 253 (1978) 716–722.
- [68] M.R. Paquet, S. Narasimhan, H. Schachter and M.A. Moscarello, Branch specificity of purified rat liver golgi UDP-galactose:*N*-acetylglucosamine  $\beta$ -1  $\rightarrow$  4-galactosyltransferase, *J. Biol. Chem.*, 259 (1984) 4716–4721.
- [69] G. Ashwell and J. Harford, Carbohydrate-specific receptors of the liver, *Ann. Rev. Biochem.*, 51 (1982) 531–554.
- [70] Y.C. Lee, R.R. Townsend, M.R. Hardy, J. Loentigren, J. Arnarp, M. Haraldsson and H. Loenn, Binding of synthetic oligosaccharides to the hepatic Gal/GalNAc lectin, *J. Biol. Chem.*, 258 (1983) 199–202.
- [71] Y.C. Lee, R.R. Townsend, M.R. Hardy, J. Loennigren and K. Bock, Binding of synthetic clustered ligands to the Gal/GalNAc lectin on isolated rabbit hepatocytes, in T.B. Lo, T.Y. Liti and C.H. Li, (eds.), *Biochemical and biophysical studies of proteins and nucleic acids*, Elsevier, New York, 1984, pp. 349–360.
- [72] H.F. Lodish, Recognition of complex oligosaccharides by the multi-subunit asialoglycoprotein receptor, *Trends Biochem. Sci.*, 16 (1991) 373–377.
- [73] D.R.P. Tulsiani and O. Touster, The purification and characterization of mannosidase IA from rat liver Golgi membranes, *J. Biol. Chem.*, 263 (1988) 5408–5417.
- [74] T.J. Rutherford, J. Partridge, C.T. Weller and S.W. Homans, Characterization of the extent of internal motions in oligosaccharides, *Biochemistry*, 32 (1993) 12715–12724.